Magnesium-containing bioceramics stimulate exosomal miR-196a-5p secretion to promote senescent osteogenesis through targeting *Hoxa7*/MAPK signaling axis

A B S T R A C T

Stem cell senescence is characterized by progressive functional dysfunction and secretory phenotypic changes including decreased proliferation, dysfunction of osteogenic and angiogenic differentiation, increased secretion of the senescence-associated secretory phenotype (SASP), which bring difficulties for bone repair. Rescuing or delaying senescence of aged bone marrow mesenchymal stem cells (O-BMSCs) was considered as effective strategy for bone regeneration in aging microenvironment. Magnesium (Mg) ion released from bioceramics was reported to facilitate bone regeneration via enhancing osteogenesis and alleviating senescence. In this study, Akermanite bioceramics (Akt) containing Mg ion as a model was demonstrated to promote osteogenesis and angiogenesis effects of O-BMSCs by activating the MAPK signaling pathway *in vitro*. Moreover, the enhanced osteogenesis effects might be attributed to enhanced Mg-containing Akt-mediated exosomal miR-196a-5p cargo targeting *Hoxa7* and activation of MAPK signaling pathway. Furthermore, the *in vivo* study confirmed that 3D-printed porous Mg-containing Akt scaffolds effectively increased bone regeneration in cranial defects of aged rats. The current results indicated that the exosomal-miR-196a-5p/*Hoxa7*/MAPK signaling axis might be the potential mechanism underlying Akt-mediated osteogenesis. The exosome-meditaed therapy stimulated by the released Mg ion contained in Akt biocreamics or other biomaterials might serve as a candidate strategy for bone repair in aged individuals.

1. Introduction

Aging, an inevitable process characterized by reduced self-renewal and multilineage differentiation and progressive functional declines, leads to the occurrence of age-related diseases [1–3]. Generally, senescence of bone marrow mesenchymal stem cells (BMSCs) exhibits the properties of decreased proliferation, dysfunction of osteogenic and angiogenic differentiation, increased secretion of the senescence-associated secretory phenotype (SASP) and pro-inflammatory factors, bringing great difficulties for bone regeneration and repair in the elderly individuals [4–8]. Bone tissue engineering including stem cells, growth factors and scaffolds has been acknowledged as the ideal strategy in promoting senescent bone regeneration [9–12]. However, stem cell therapies and growth factors have various limitations, such as a lack of suitable sources of donor cells, adverse immunological rejection, difficulty of controlled delivery and tumorigenicity [13–16]. Recently, it was reported that the ions released from biomaterials have the function of promoting proliferation and osteogenic differentiation of BMSCs to accelerate bone regeneration [17–19]. For example, strontium ion could rebalance bone marrow adipogenesis and osteoblastogenesis in SAMP6 mice, a senescent murine model, through NFATc/Maf and Wnt signaling [20]; The literature also

indicated that the release of magnesium ion (Mg) contained in titanium implants could promote rapid bone formation and the activation of osteogenic signals in osteoporotic mice [21]. Therefore, it was of great importance to develop and design a novel biomaterial scaffold containing special chemical ions that could rescue the function of senescent BMSCs and overcome the above obstacles to promote bone regeneration under senescent status.

It was reported that Mg ion play essential roles in the process of bone formation via promoting osteogenesis and angiogenesis [22–26]. Akermanite ($Ca_2MgSi_2O_7$) bioceramics (Akt) containing the ions of Ca, Mg and Si have been proven to promote osteogenic differentiation, wound healing, angiogenesis and osteochondral regeneration because of their properties of slowly releasing these ions [27–30]. In addition, Mg-containing Akt combined with other components to form biological scaffolds could improve its positive biodegradability and bioactivity to further promote bone repair. For example, previous literature has reported that 3D-printed porous iron-based composites containing Akt scaffold enhanced proliferation and osteogenic differentiation of BMSCs to stimulate bone mineralization [31]. More importantly, Mg-containing Akt exhibits a superior bone regenerative performance in the process of the treatment of osteoporotic bone defect [32]. Our previous study also indicated that Ti–6Al–4V implants coated by a nano-structured Akt

could improve new bone formation and osseointegration of osteoporosis, an age-related bone metabolic disease model [33]. Therefore, Akt containing the special chemical ions of Mg was expected to promote osteogenesis of O-BMSCs. However, its detailed effects and the potential mechanisms remain to be systematically investigated in O-BMSCs with complicated aging microenvironment.

In addition to the canonical signaling pathway, exosomes, 30–150nm extracellular vesicles, have recently emerged as novel mediators for their properties of rich contents, low immunogenicity and safety through paracrine and autocrine functions [34–38], which regulate osteogenesis and angiogenesis through delivering their cargoes [39, 40]. For example, exosomes isolated from umbilical mesenchymal stem cells promoted angiogenesis via the miR-21/NOTCH1/DLL4 signaling axis to further accelerate bone repair [41]; BMSC-derived exosomes derived from osteoinductive media combined with hierarchical mesoporous bioactive glass (MBG) scaffold improve bone regeneration of critical defects [42]. It is well recognized that the alternations of cell culture microenvironment could modulate the exosomal cargoes of producing cells, which would therefore further affect the biological functions of targeted cells [43,44]. Exosomes derived from BMSCs cultured in Sr-CS extracts have been observed to promote osteogenesis and angiogenesis through delivering miR-146a that suppresses Smad4 and NF2 pathways [45]. However, whether Akt regulate osteogenesis and angiogenesis in an aging microenvironment through modulating exosome secretion has not been elucidated. In addition, the miRNAs packaged into exosomes as signal regulators between cells and the downstream mechanisms mediated by Akt-mediated exosomes remained largely unknown.

Therefore, this study analyzed the impacts of Mg-containing Akt on the osteogenesis and angiogenesis of O-BMSCs *in vitro* with β-tricalcium phosphate (β-Ca$_3$(PO4)$_2$, β-TCP) and calcium silicate (CS) bioceramic as the control group. The previously reported MAPK signaling pathway was explored to observe its roles in Mg-containing Akt-mediated osteogenesis. Moreover, the biological functions of exosomes derived from O-BMSCs stimulated by Mg-containing Akt were isolated and investigated. In addition, exosomal miRNAs sequencing was performed to screen the candidate exosomal miRNAs involved in Mg-containing Akt-mediated osteogenesis and angiogenesis. The potential target genes and downstream signaling pathways were predicted to further clarify the detailed mechanisms. Moreover, 3D-printed Mg-containing Akt scaffolds were prepared and implanted into aged rats' calvarial critical defects to further evaluate their pro-osteogenesis *in vivo* under the senescent microenvironment.

2. Results and discussion

2.1. Characterization of materials

The prepared Akt, CS and β-TCP specimens were demonstrated by FTIR and XRD analysis. The FTIR spectra of the Akt, CS and β-TCP specimens were shown in Figs. S1A–C. The FTIR analysis of the β-TCP sample demonstrated the stretching mode of PO4^{3-} which formed a strong band observed at 1044 cm^{-1}. The vibration peaks of PO4^{3-} were observed at 552 cm^{-1}, and 610 cm^{-1}. The FTIR analysis of the CS sample demonstrated the tetrahedral symmetrical stretching vibration (Si=O) and nonbridged oxygen stretching vibration (Si=O) were from 500 to 900 cm^{-1}. The waves of anti-symmetric stretching vibration of Si=O=Si bond in the SiO4 tetrahedra was from 900 to 1200 cm^{-1}. The FTIR spectra of the Akt sample obtained showed the O–Mg–O bending modes at 485 cm^{-1}. The Ca=O group has a band at 585 cm^{-1}, while the O–Si–O bands have occurred at 635 cm^{-1} and 681 cm^{-1}. The bandsat 849 cm^{-1}, 931 cm^{-1} and 970 cm^{-1} illustrate the Si=O stretching modes. The symmetric stretching at 1007 cm^{-1} was assigned to the Si=O=Si vibration. From the diffraction peaks of XRD, the results confirm that the prepared materials were β-TCP (JCPDS file No. 09-169), CS (JCPDS file No. 43-1460) and Akt (JCPDS file No. 01-077), respectively

(Figs. S1D–1F). The ICP-AES results of various diluted extracts were provided in Figs. S1G–1I. The results indicated that the Ca ion showed no significant changes among various diluted extracts. The Si ion in CS extracts was higher than that in Akt extracts, which might attribute to the different rates in degradation, while Si ion was almost absent in β-TCP extracts. The Mg ion was within the range of 0.8–3.2 mg/L in 1/16-1/64 dilutions of Akt extracts, while Mg ion was absent in β-TCP and CS extracts. In addition, surface pH values of various kinds of materials were recorded. As illustrated in Fig. S1J, Akt (pH 9.15 ± 0.12) generated a higher pH value than those of calcium silicate (CS) (pH 8.45 ± 0.12) and β-TCP (pH 7.42 ± 0.12). Then, the surface pH values of each material were dropped to lowest point (8.57 ± 0.13 for Akt; 7.70 ± 0.11 for CS; 7.35 ± 0.16 for β-TCP) 1 day after the immersion. After that, the surface pH values of these materials were gradually increased and reached relatively stable value at 3–7 days. The SEM results demonstrated that the 3D-printed β-TCP and Akt bioceramic scaffolds exhibited porous structures connected by uniformly distributed pores of the same size (Fig. S1K-1L). The changes in the ions content of Akt scaffolds were presented in Fig. S1M-1O. It was obvious that the content of the Ca, Mg, and Si from Akt scaffolds increased with the increase in soaking time, which indicated that the controlled release of these special ions with degradation of scaffolds. These results demonstrated that the Akt or β-TCP extracts or scaffolds were successfully prepared to conduct the following experiments.

Recently, Mg has attracted growing attention due to its perfect biocompatibility, biodegradability and low levels of toxicity in medical research [46]. Previous studies shown that Mg^{2+} could increase osteogenic activity and decrease osteoclasts activity, consequently accelerating bone formation [47,48]. Besides, Mg could prevent inflammation and mediate autophagy to promote osteogenesis by interfering with macrophage-derived exosomes [49]. In addition to the released Mg, alkaline microenvironment pH (μe-pH) was also an important positive factor for bone regeneration. The previous study has revealed that the pH influenced by different materials was sufficient to affect osteoclast behaviors independently of the released ions, which play important roles at the early stage of bone defect regeneration [50]. In addition, Akt was demonstrated to exhibit a durable μe-pH in osteoporotic bone defect healing process that might lead to greater bone repair [32]. Therefore, in addition to the anabolic effect of the released Mg, the weak alkaline μe-pH provided by Akt was expected to show positive effects on osteogenic differentiation.

2.2. Akt extracts mediate proliferation and osteogenesis of O-BMSCs

The proliferation ability of O-BMSCs after treatment with gradient concentrations of Akt and β-TCP extracts was compared using the CCK-8 assay. It was clear that the extracts could apparently promote the proliferation of O-BMSCs from 1/8 to 1/32 dilution (Fig. 1A). Moreover, the optimal pro-proliferation effect was observed at the 1/32 diluted concentration. The OD value of the Akt extract group showed significant differences in comparison to the β-TCP extract and control group. Therefore, the appropriate concentration was set at 1/32 dilution of extracts to perform the following experiments (Fig. 1B).

The expression of osteogenesis-, angiogenesis- and senescence-related genes of O-BMSCs cultured in the Akt and β-TCP extracts at days 4, 7 and 10 were detected by qRT-PCR analysis. As shown in Fig. 1C–G, the results demonstrated that Akt extracts could promote the gene expression of *Alp* and *Ocn* in O-BMSCs compared to the medium alone and β-TCP extracts at days 4. In addition, it was clear that Akt extracts promoted osteogenesis-related gene expression including *Alp*, *Ocn* and *Runx2* at days 7. The results also demonstrated that Akt extracts promoted osteogenesis-related gene expression including *Alp*, *Col-1* and *Ocn* at days 10. Moreover, the Akt extracts also upregulated the expression of angiogenesis-related genes, including *Ang-1* and *Vegf* (Figs. S2A–2B) in O-BMSCs. The osteogenic differentiation and senescence of O-BMSCs in different extract groups were further detected via
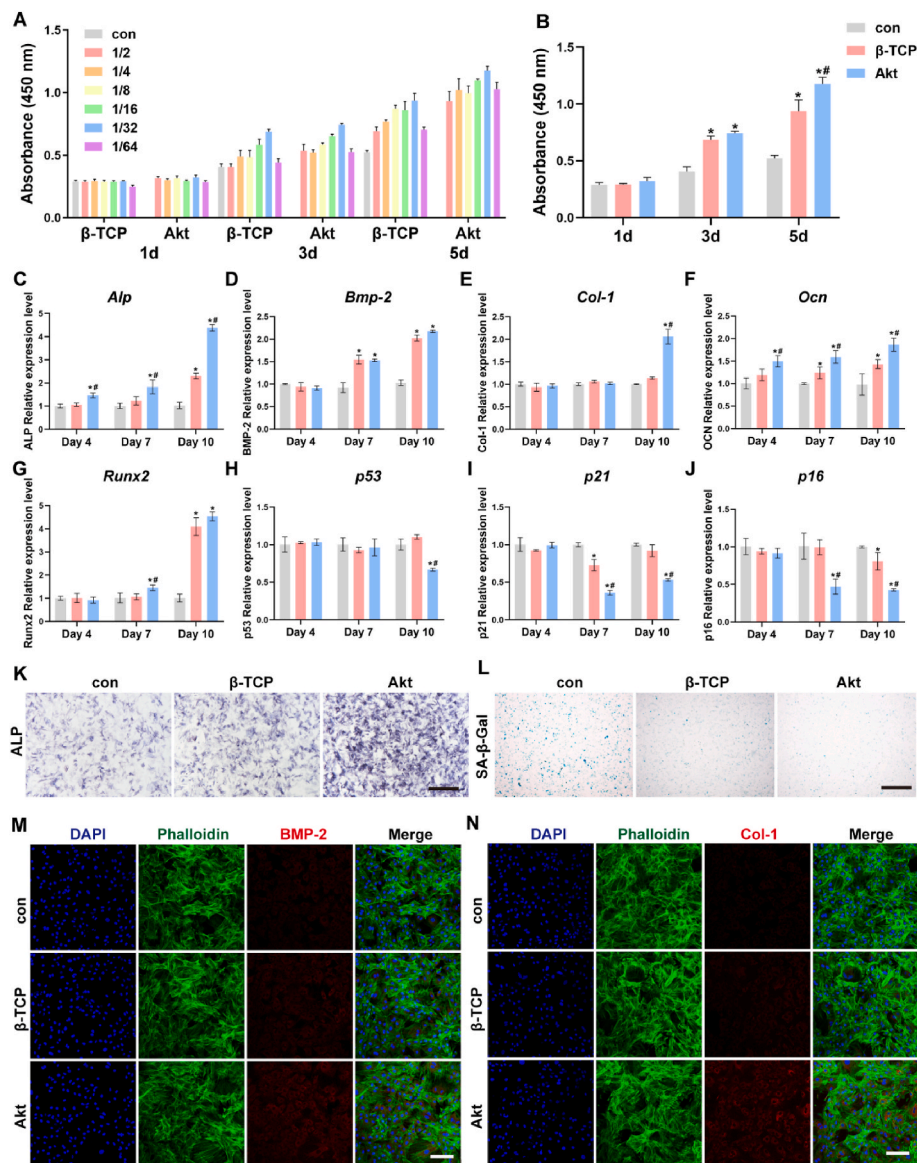
Fig. 1. Akt extracts promote proliferation and osteogenesis of O-BMSCs. (A) CCK8 assay for the proliferation of O-BMSCs cultured in different concentrations of Akt and β-TCP extracts. (B) The suitable concentration of 1/32 dilution of Akt and β-TCP extracts on cell proliferation of O-BMSCs. (C–J) qRT-PCR analysis of osteogenesis-related genes *Alp* (C), *Bmp-2* (D), *Col-1* (E), *Ocn* (F), *Runx2* (G) and senescence-related genes *p53* (H), *p21* (I) and *p16* (J) cultured in 1/32 dilution of Akt and β-TCP extracts at days 4, 7 and 10. (K–N) The ALP staining (K), SA-β-Gal staining (L) and immunofluorescence staining of osteogenesis-related proteins Bmp-2 (M) and Col-1 (N) for O-BMSCs cultured in 1/32 dilution of Akt and β-TCP extracts. cultured in 1/32 dilution of Akt and β-TCP extracts.. (*indicates significant differences compared with medium; #indicates significant differences compared with β-TCP extracts, $p < 0.05$. Scale bar, 100 μm.)

ALP and SA-β-gal staining. As shown in Fig. 1K, ALP staining results showed that Akt extracts induced higher ALP activity compared to the medium alone and β-TCP extracts. ARS staining also showed that the osteogenic differentiation was increased after treatment with Akt extracts (Fig. S2C). The SA-β-gal positive cells significantly decreased after treatment with the Akt extracts when compared with those treated with the β-TCP extracts or control medium (Fig. 1L). The expression of osteogenic proteins, including Bmp-2 and Col-1, were increased when treated with the Akt extracts, as detected by immunofluorescence staining (Fig. 1M–N).

To exclude the potential influence of released Si ion from the Akt, CS was chosen as an additional control to investigate its effects in O-BMSCs under the same concentration. As indicated in Fig. S3A, all the extracts (1/32 dilution) could promote proliferation of O-BMSCs. Akt extract induced higher proliferative capacity compared to CS or β-TCP extract. ALP staining also demonstrated that Akt extract was more effective in

promoting osteogenic differentiation compared to CS or β-TCP extract (Fig. S3B). The trend of ALP staining in Y-BMSCs was similar to that in O-BMSCs. In addition, the osteogenic-related genes including *Alp*, *Bmp-2*, *Col-1*, *Ocn* and *Runx2* were significantly increased after treatment with Akt extracts compared to the cells treated by CS or β-TCP extract (Figs. S3C–3G). In contrast, Akt extract downregulated the aging-related genes including *p53*, *p21* and *p16* compared to CS extract though these genes shown a certain degree of reduction after treatment with CS extract (Figs. S3H–3J). The angiogenic-related genes including *Ang-1* and *Vegf* in O-BMSCs were also significantly upregulated after treatment with treatment with Akt extracts compared to the cells treated by CS or β-TCP extracts (Figs. S4A–4B). The trend of angiogenesis potential was also exhibited in Y-BMSCs (Figs. S4C–4D). In addition, the migration was significantly increased in O-BMSCs and Y-BMSCs treated with Akt extracts compared with those treated with CS or β-TCP extracts (Figs. S4E–4F). Though the migration were all increased after treatment

with every extracts. Hence, under the exclusion of interference from Si ion, the above results demonstrated that the Mg-containing Akt extracts could promote the proliferation, migration, osteogenic and angiogenic differentiation and alleviated senescence-related phenotypes of O-BMSCs.

Senescence would break the balance between mineralization and resorption regulated by osteoblasts and osteoclasts, respectively, at the cellular level, ultimately leading to aging-related osteoporosis [51–54]. Therefore, it is of great importance to rejuvenate the senescent BMSCs, precursor cells of osteoblasts, in age-related bone diseases. Recently, ceramic biomaterilas containing special chemical elements have exhibited great potential in the field of bone repair [55–58]. Mg plays an important role in promoting bone growth and regeneration [59–62]. For instance, a recent study reported that Mg-ion-modified black

phosphorus (BP) nanosheets could promote osteogenesis and angiogenesis, further causing vascularized bone regeneration [63]. In addition, the 3D-printed Mg-doped β-TCP gyroid scaffold possessed a satisfying bone defect repair capability by promoting osteogenesis and angiogenesis [64]. Our previous study also demonstrated that Akt bioceramics containing Mg promote osteogenesis and angiogenesis while inhibiting osteoclast formation in the OVX-BMSC model through MAPK signaling pathway [65]. In the our present study, we chosen β-TCP and CS as control ceramic to exclude the interference of Ca and Si to further investigate the effects of the Mg-containing Akt in aging microenvironment. Altogether, the study demonstrated that Akt bioceramics containing Mg could promote the proliferation, migration, osteogenic and angiogenic differentiation and alleviated senescence-related phenotypes of O-BMSCs. However, the regulated mechanism of Mg
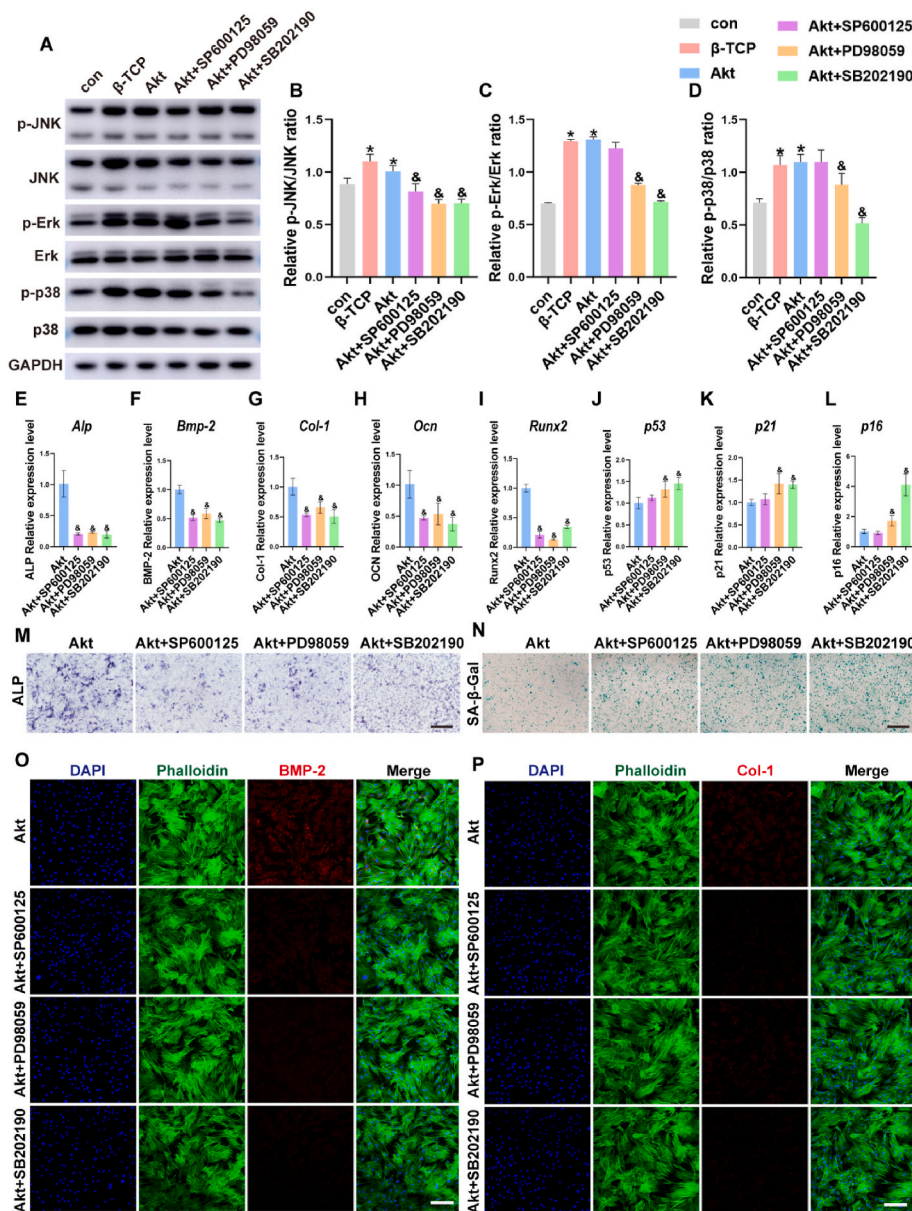

Fig. 2. MAPK pathway play a role in Akt-mediated osteogenesis of O-BMSCs. (A) Western blotting assay for key proteins expression of MAPK pathway for O-BMSCs treated with β-TCP extracts, Akt extracts and inhibitors SP600125 (JNK), PD98059 (Erk) and SB202190 (p38). (B–D) The quantitative assay for the ratios of p-JNK/JNK (B), p-Erk/Erk (C), p-p38/p38 (D). (E–L) qRT-PCR analysis of osteogenesis-related genes *Alp* (E), *Bmp-2* (F), *Col-1* (G), *Ocn* (H), *Runx2* (I) and senescence-related genes *p53* (J), *p21* (K) and *p16* (L) cultured in Akt extracts with inhibitors SP600125, PD98059 and SB202190. (M−P) The ALP staining (M), SA-β-Gal staining (N) and immunofluorescence staining of osteogenesis-related proteins Bmp-2 (O) and Col-1 (P) for O-BMSCs cultured in Akt extracts with inhibitors SP600125, PD98059 and SB202190. (*indicates significant differences compared with medium. &indicates significant differences compared with Akt extracts, $p < 0.05$. Scale bar, 100 μm.)

containing Akt biomaterilas remain unclear.

2.3. MAPK pathway plays a role in Akt-mediated osteogenesis of O-BMSCs

MAPK signaling is one of the essential pathways in the field of bone tissue engineering, which prompted us to further explore these effects and the potential mechanisms in O-BMSCs. To further examine whether the previously reported MAPK pathway in OVX-BMSCs was also responsible for Akt-mediated osteogenesis and angiogenesis in O-BMSCs, the p-Erk, p-JNK, and p-p38 protein expressions were detected after treatment with the Akt and β-TCP extracts. Also, the p38 inhibitor (SB202190), Erk inhibitor (PD98059) and JNK inhibitor (SP600125) were applied to further confirm the involvement of JNK, Erk and p38 pathways in Akt-mediated osteogenesis of O-BMSCs. The Western blot results showed that the expressions of phosphorylate JNK and Erk and p38 were significantly enhanced after treatment with the Akt extracts and the β-TCP extracts (Fig. 2A–D). Enhanced p-JNK, p-Erk and p-p38 could be critically inhibited by SP600125, PD98059 and SB202190, respectively. Also, the Western blot analysis also demonstrated a mutual

inhibition between these inhibitors. For example, the JNK inhibitor SP600125 could suppress the activation of p-Erk and p-p38. And the Erk inhibitor PD98059 could decrease the expression of p-p38, while p38 inhibitor SB202190 also inhibited the expression of p-Erk. To further confirm the involvement of JNK, Erk and p38 pathways in Akt-mediated osteogenesis and angiogenesis, the signaling pathway inhibition assay was then performed. The results clearly shown that the upregulated expression of osteogenic-related genes including *Alp, Bmp-2, Col-1, Ocn* and *Runx2* (Fig. 2E–I) and angiogenic-related genes such as *Ang-1* and *Vegf* (Figs. S5A–5B) can be compromised by JNK, Erk and p38 inhibitors. And the senescent-related genes p53, p21 and p16 displayed opposite tendencies (Fig. 2J–L). Moreover, ALP staining results indicated that the enhanced osteogenic ability was also partially inhibited by the pathway inhibitors to some extent (Fig. 2M). ARS staining also demonstrated that the osteogensis stimulated by Akt extract was compromised by these pathway inhibitors (Fig. S5C). In contrast, SA-β-gal staining demonstrated that the number of positive staining cells was increased after treatment with the Akt extracts followed by the three inhibitors (Fig. 2N). The expression of osteogenic proteins, including Bmp-2 and Col-1, were also blocked by the three inhibitors, as revealed by cell
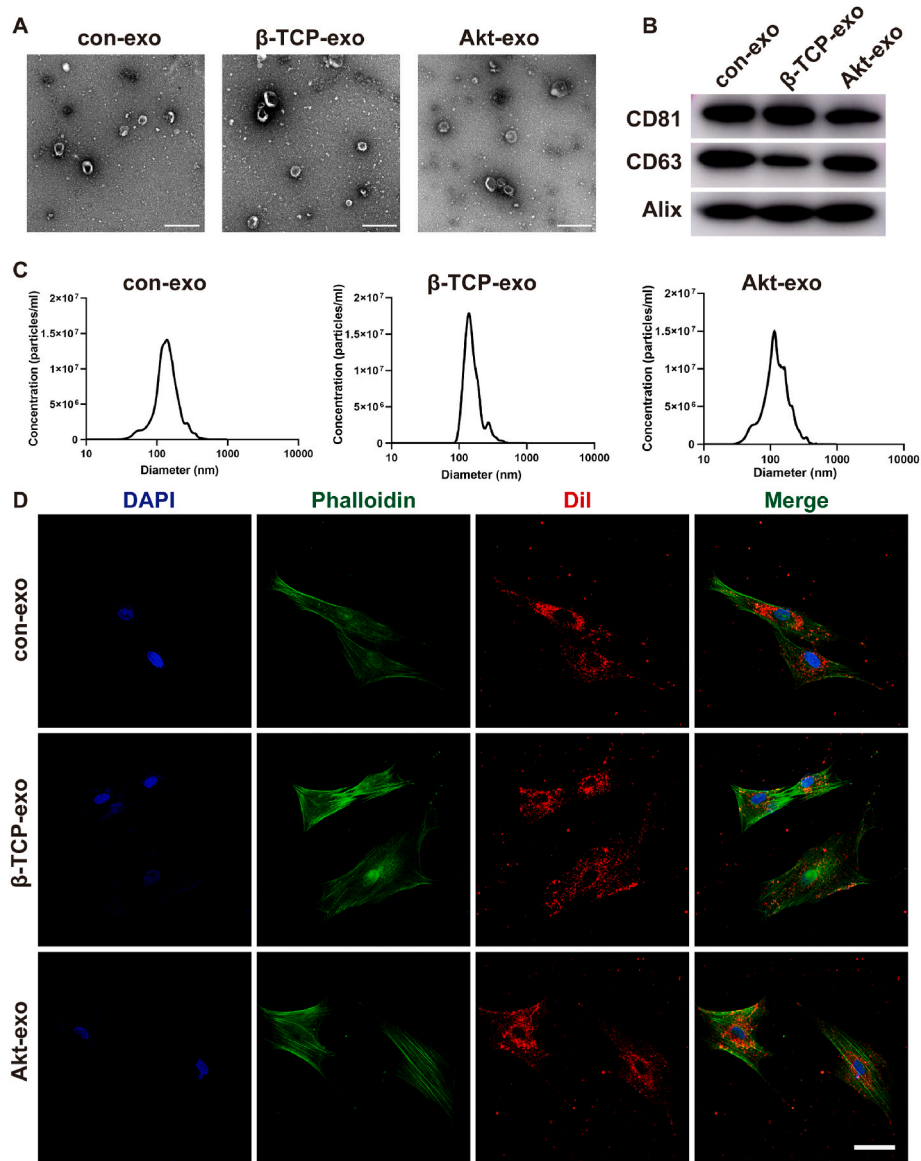

Fig. 3. Characterization and internalization of exosomes. (A) TEM images of exosomes. Scale bar, 500 μm. (B) Western blotting assay for exosome markers CD81, CD63 and Alix. (C) NTA analysis for particle size distribution of exosomes. (D) The internalization of Dil-labeled exosomes by O-BMSCs. Scale bar, 100 μm.

immunofluorescence staining (Fig. 2O, P). These results suggested that the MAPK pathways might play an indispensable role in Akt-mediated osteogenesis, angiogenesis, and senescence of O-BMSCs.

2.4. Akt-exo mediates osteogenesis of O-BMSCs

In addition to the conventional MAPK signaling pathways, recent studies have demonstrated that paracrine mechanisms was also significant for bone regeneration [66–68]. Mounting evidences have demonstrated that exosomes as the upstream paracrine mediators of MAPK signaling pathways between cells could deliver rich contents to mediate different kinds of physiological and pathological conditions, including bone tissue regeneration [69–73]. Hence, the exosome stimulated by Akt or β-TCP extracts was isolated and purified to further explore its effect on O-BMSCs.

As illustrated in Fig. 3A, TEM indicated that the exosomes were 50–150nm membrane-bound and cup-shaped vesicles. The exosomal-specific markers including CD81, CD63 and Alix could be observed in different exosomes (Fig. 3B). The size distribution of different exosomes exhibited single bell-shapes and peaked at approximately 150nm (Fig. 3C). Notably, the shape and diameter had no significant difference between different exosomes, indicating that different extracts had no influence on the production and isolation of exosomes. To examine the internalization of different exosomes, the O-BMSCs were treated with exosomes labeled with red fluorescent dye Dil for 12h. As shown in

Fig. 3D, Dil-labeled exosomes were distributed near the nucleus of O-BMSCs. Analysis demonstrated that the uptake of exosomes had no different significance between groups (Fig. S6).

To further explore the effects of Akt-exo on O-BMSCs, proliferation and osteogenic differentiation of O-BMSCs under different exosome stimulation were evaluated. Firstly, the CCK-8 assay was performed to compare the effect of gradient concentrations (50μg/ml, 100μg/ml, 150μg/ml, 200μg/ml) of different exosomes on the proliferative ability of O-BMSCs. As shown in Fig. 4A, the results revealed that all types of exosome, including con-exo, β-TCP-exo and Akt-exo, displayed promotional effects from the concentration of 50μg/ml to 150μg/ml, and 150μg/ml exosomes induced the highest OD values, which indicated the O-BMSCs exhibited the highest proliferative capacity at this concentration. Therefore, 150μg/ml was chosen in the following studies. It was clear that Akt-exo could promote the proliferation of O-BMSCs at days 1, 3 and 5 compared to con-exo and β-TCP-exo at a concentration of 150 μg/ml (Fig. 4B). The qRT-PCR assay demonstrated that the expressions of osteogenic genes, including *Alp*, *Bmp-2*, *Col-1*, *Ocn* and *Runx2* (Fig. 4C–G), and angiogenic genes, *Ang-1* and *Vegf* (Figs. S7A–7B), were substantially upregulated by Akt-exo stimulation compared to con-exo or β-TCP-exo. However, the expressions of aging-related genes including *p53*, *p21* and *p16* (Fig. 4H–J) and pro-inflammatory factors including *IL-1β*, *IL-6* and *Tnf-α* (Figs. S7C–7E), were significantly downregulated after treatment with Akt-exo compared to con-exo or β-TCP-exo, although β-TCP-exo could also ameliorate the senescent
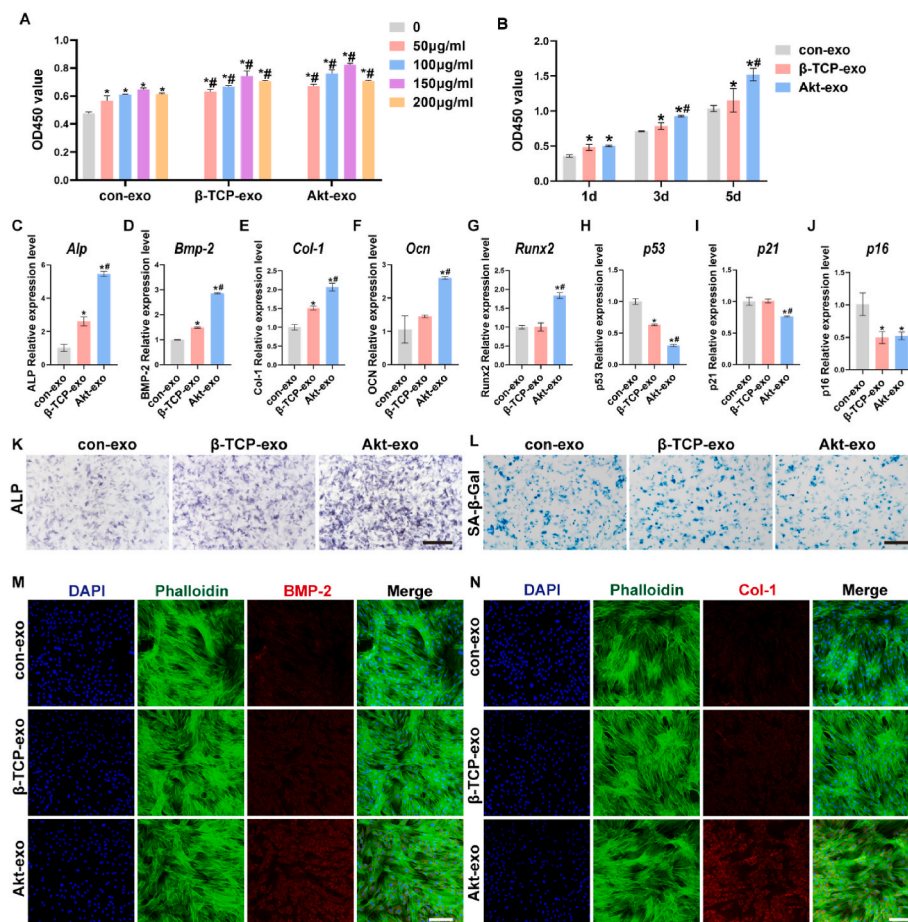

Fig. 4. Akt-exo promotes osteogenesis of O-BMSCs. (A) CCK8 assay for O-BMSCs cultured in exosomes at different concentrations at day 3. (*indicates significant differences compared with the blank control (0); #indicates significant differences compared with con-exo. $p < 0.05$.) (B) CCK8 assay for O-BMSCs cultured in exosomes at the concentration of 150 μg/ml at days 1, 3 and 5. (C–J) qRT-PCR analysis of osteogenesis-related genes *Alp* (C), *Bmp-2* (D), *Col-1* (E), *Ocn* (F), *Runx2* (G) and senescence-related genes *p53* (H), *p21* (I) and *p16* (J) cultured in exosomes. (K–N) The ALP staining (K) and SA-β-Gal staining (L) and the immunofluorescence staining of osteogenesis-related proteins Bmp-2 (M) and Col-1 (N) for O-BMSCs cultured in different types of exosomes. (*indicates significant differences compared with con-exo; # indicates significant differences compared with β-TCP-Exo, $p < 0.05$. Scale bar, 100 μm.)

phenotypes of O-BMSCs to some extent. In addition, Akt-exo markedly promoted the osteogenic differentiation of O-BMSCs, while β-TCP-exo could also improve osteogenesis to a certain degree, as shown by the results of the ALP staining (Fig. 4K). ARS staining also demonstrated that Akt-exo significantly promote osteogenic differentiation (Fig. S7F). Moreover, SA-β-gal staining manifested that compared with con-exo or β-TCP-exo, Akt-exo decreased the positive staining cells, which meant that Akt-exo delayed the aging process of O-BMSCs (Fig. 4L).

Furthermore, cell immunofluorescence staining confirmed that the expressions of osteogenic-related proteins, Bmp-2 and Col-1, were significantly increased when treated with Akt-exo (Fig. 4M–N). Collectively, the above results validated that Akt-exo could promote the proliferation and osteogenic differentiation and ameliorate the senescent phenotypes of O-BMSCs *in vitro,* which presented similar trends to Akt extracts.

Recently it has been suggested that exosomes play essential roles in reversing some degenerative, age-related diseases, which was therefore
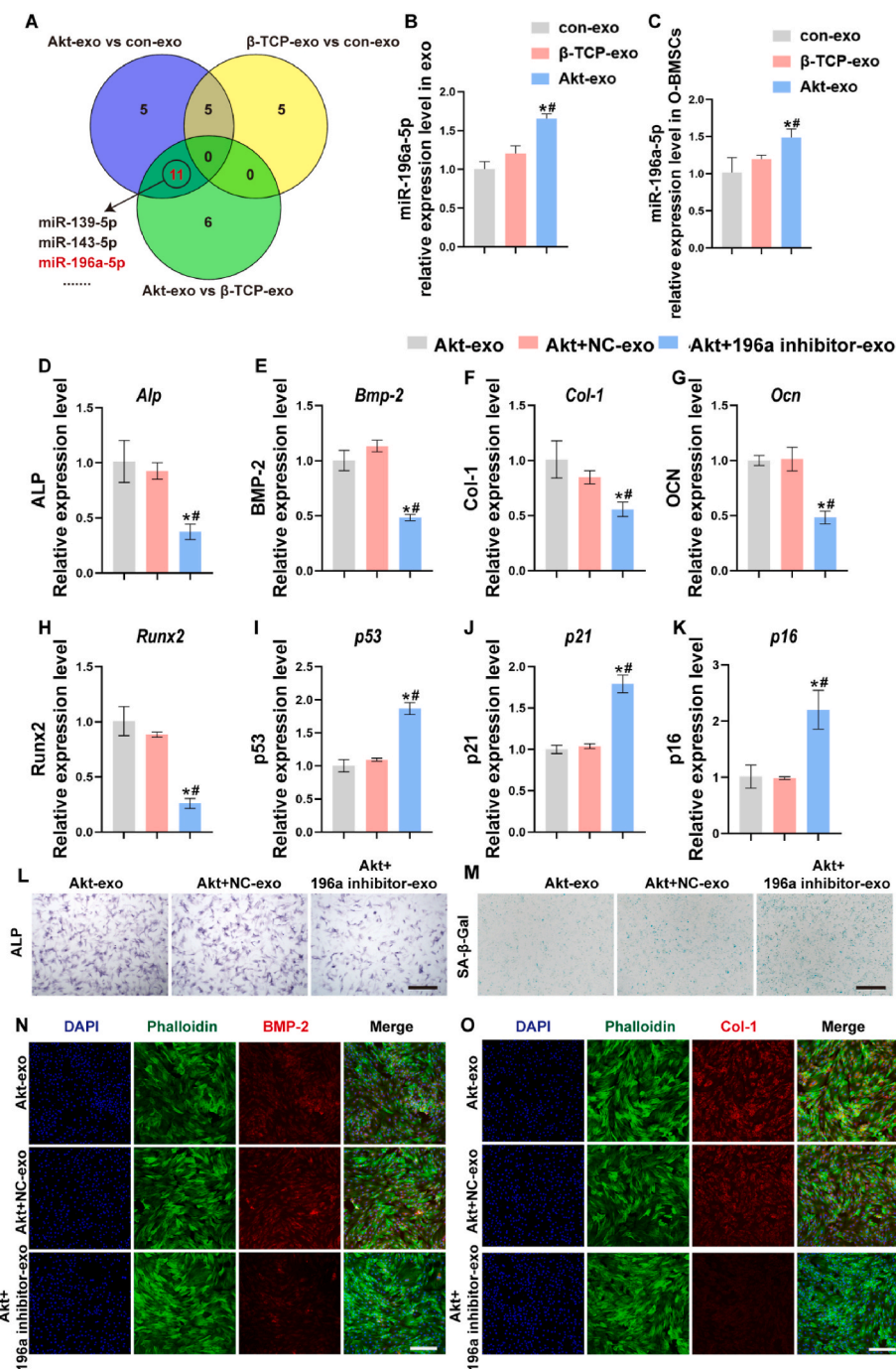

Fig. 5. Exosomal miR-196a-5p is involved in Akt-exo mediated osteogenesis of O-BMSCs. (A) Screening of exosomal miR-196a-5p by exosomal miRNA sequencing. (B–C) qRT-PCR analysis for the expression levels of miR-196a-5p in different types of exosomes (B) and in O-BMSCs treated with different types of exosomes (C). (*indicates significant differences compared with con-exo; # indicates significant differences compared with β-TCP-exo, $p < 0.05$.) (D–L) qRT-PCR analysis of osteogenesis-related genes *Alp* (D), *Bmp-2* (E), *Col-1* (F), *Ocn*(G), *Runx2* (H) and senescence-related genes *p53* (J), *p21* (J) and *p16* (K) for O-BMSCs cultured in different types of exosomes. (L–M) The ALP staining (L), SA-β-Gal staining (M) and the immunofluorescence staining of osteogenesis-related proteins Bmp-2 (N) and Col-1 (O) for O-BMSCs cultured in different types of exosomes.. (*indicates significant differences compared with Akt-exo; # indicates significant differences compared with Akt + NC-Exo, $p < 0.05$. Scale bar, 100 μm.)

recognized as the promising strategy for promoting bone regeneration [74–76]. Previous study have demonstrated that the microenvironment and culture medium might alter the functions of the cells by affecting the secreted exosome cargo of host cells. For instance, the study indicated that the angiogenic ability of HUVECs was noticeably upregulated by Li-BGC, during which the transfer of exosomes derived from Li-BGC-stimulated BMSCs was proposed as the key mechanism [77]. However, whether the paracrine functions of the exosome played important roles in the process of Akt-mediated osteogenesis of O-BMSCs was less studied. The isolated exosomes stimulated by Akt extracts in this study alleviated senescence, enhanced proliferation and osteogenesis of O-BMSCs, which added to the proofs that Akt-mediated osteogenesis was related to the exosomes secretion. In addition, there is no difference in the production and exosomal uptake of exosomes stimulated by different extracts. Hence, we speculated that the positive promoting effects of Akt-exo on O-BMSCs might be attributed to the special cargoes in exosomes that could transfer to recipient cells, which eventually increased osteogenesis and angiogenesis. Of note, CS-exo was not included in the present study. Based on the above results, we speculated that Akt-exo would exhibited greater potential in osteogenic and angiogenic differentiation than CS-exo. To address this issue, the detailed effects of CS-exo on O-BMSCs would be performed in the future study.

2.5. Exosomal miR-196a-5p is involved in Akt-exo-mediated osteogenesis

Previous studies have demonstrated that miRNAs were abundant in exosomes, which played important roles in various bone-related diseases. For example, miR-5106 enriched in M2 macrophage-derived exosomes induce osteogenic differentiation through targeting SIK2 and SIK3 [78]; ADSCs-Exo effectively regulate bone healing and maintain immune metabolism via miR-451a/MIF signaling axis [79]. Hence, it is of great importance to clarify the miRNAs contained in exosomes that regulate osteogenesis and reverse senescence of O-BMSCs in our present study. In this study, to identify the candidate miRNAs involved in Akt-exo-mediated osteogenesis and angiogenesis, the con-exo, β-TCP-exo and Akt-exo were isolated and subjected to exosomal miRNA sequencing (Figs. S8A–8C). As indicated in Fig. 5A, we first intersected the differential genes of Akt-exo *vs* β-TCP-exo and Akt-exo *vs* con-exo to screen the candidate miRNAs. The detailed expression of the 11 filtered miRNAs were provided in Supplementary Table 2. After reviewing the literature, miR-1306-5p, miR-143-5p, miR-296-3p, miR-30c-2-3p, miR-322-3p, miR-351-3p, miR-365-5p, miR-493-3p and miR-434-3p were seldom reported to be related to osteogenesis and angiogensis of BMSCs. miR-139-5p was reported to repress osteogenesis of BMSCs via targeting Wnt/β-Catenin Signaling Pathway [80,81]. In addition, miR-139-5p inhibited tube formation, migration, proliferation, and down-regulated the expression of angiogenesis-related genes in HUVECs and ECFCs [82]. The study also demonstrated that senescent osteoblast-derived exosome-mediated miR-139-5p could promote the senescence and apoptosis and inhibit their proliferation and migration of vascular endothelial cells [83]. Therefore, miR-139-5p was reported to be negatively related to osteogenesis and angiogenesis. However, miR-196a-5p was reported to own the differentiation potential of the paraxial mesodermal cells into skeletal muscle lineage [84]. In addition, the other study has indicated that the decrease in miRNA-196a-5p may be important in steroid-induced osteonecrosis of the femoral head [85]. Therefore, miR-196a-5p was specifically selected to perform the following experiments to investigate its effects on osteogenesis and angiogenesis of O-BMSCs in this present study.

As seen in Fig. 5B, miR-196a-5p in Akt-exo showed a higher expression than in β-TCP-exo and con-exo in O-BMSCs. In addition, in Y-BMSCs, miR-196a-5p in Akt-exo showed similar trend compared to β-TCP-exo and con-exo. The comparison between O-Akt-exo and Y-con-exo was already close, although it showed statistically significant, which indicate that Akt-exo exhibited positive rejuvenation of O-BMSCs to

some extent (Fig. S8D). More notably, when compared to other groups, the expression of miR-196a-5p in O-BMSCs was considerably elevated following treatment with Akt-exo (Fig. 5C). To exclude the interference of Akt extracts stimulation directly, the expression of miR-196a-5p in O-BMSCs was compared after treatment with Akt-exo and Akt extracts directly. The results indicated that the miR-196a-5p was significantly increased after treatment with Akt-exo compared to that after treatment with Akt extracts directly though the gene expression in O-BMSCs was increased to some extent stimulated by Akt extracts (Fig. S8E). To further investigate the function of exosomal miR-196a-5p on O-BMSCs, the miR-196a-5p inhibitor was developed and transfected followed by co-culturing with Akt extracts. qRT-PCR assay demonstrated that miR-196a-5p was significantly downregulated after transfection with a miR-196a-5p inhibitor followed by Akt extracts in O-BMSCs (Fig. S8F). In addition, from Fig. S8G, it could be observed that the corresponding isolated exosome (Akt+196a inhibitor-exo) showed a drastically downregulated miR-196a-5p compared to those in exosomes transfected with the inhibitor control (Akt-exo and Akt + NC-exo). Based on this, the effect of different exosomes isolated from miR-196a-5p inhibitors or inhibitor NC followed by Akt extracts was detected. qRT-PCR demonstrated that the expression of osteogenic-related genes including *Alp*, *Bmp-2*, *Col-1*, *Runx2*, and *Ocn* (Fig. 5D–H) and angiogenic-related genes *Ang-1* and *Vegf* (Figs. S8H–8I) was obviously downregulated after treatment with Akt+196a inhibitor-exo. However, senescent-related genes, including *p53*, *p21* and *p16*, were typically upregulated in the Akt+196a inhibitor-exo group (Fig. 5I–K). ALP staining results showed that Akt+196a inhibitor-exo also inhibited osteogenic differentiation ability of O-BMSCs (Fig. 5L). ARS staining also indicated that Akt+196a inhibitor-exo inhibited osteogenesis of O-BMSCs (Fig. S8J). However, SA-β-Gal-positive cells were drastically increased when the O-BMSCs were stimulated by Akt+196a inhibitor-exo (Fig. 5M). Similarly, the expression of osteogenic-related proteins, Bmp-2 and Col-1, was significantly decreased after cell culturing with Akt+196a inhibitor-exo, as detected by cell immunofluorescence staining (Fig. 5N, O). Taken together, the results demonstrated that miR-196a-5p inhibitors could offset the promoting effect of Akt-exo on osteogenesis and angiogenesis, which suggested that miR-196a-5p transferred through exosomes and then contributed greatly to Akt-exo-mediated osteogenesis and angiogenesis of O-BMSCs.

Previous study revealed that miR-196a-5p played important roles in the development of the skeletal system via target genes, such as *HOXC8*, located within the *HOXC* gene cluster proximal to *MIR196A2*, which indicated the biological relevance of miR-196a-5p to bone morphology [86]. Other study has demonstrated that miR-196a-5p overexpression in wharton's jelly umbilical cord stem cells could promote osteogenesis and new bone regeneration in rat calvarial bone defects via Serpin Family B Member 2 (SERPINB2) [87]. In addition, LOXL1-AS1 has been found to sponge miR-196a-5p to mediate Hmga2 expression to regulate osteogenic and adipocytic differentiation of BMSCs [88]. More importantly, the study has also demonstrated that exosomal miR-196a-5p derived from C2C12 myoblasts could suppress osteoclast-like cell formation and mitochondrial energy metabolism but enhance osteoblastic differentiation in mouse cells, suggesting that it might be the potential mechanism of muscle/bone interaction [89]. Altogether, based on the literature review above, miR-196a-5p could promote osteogenesis through the downstream target genes. In our present study, we proposed that exosomal miR-196a-5p transport between cells played important roles in the process of Akt-exo mediated osteogenesis and angiogenesis. However, the potential mechanism of enchaned exosomal miR-196a-5p still needed further elucidation.

2.6. Exosomal miR-196a-5p mediates osteogenesis via targeting Hoxa7

It is well recognized that miRNAs, non-coding RNAs, usually work by inhibiting their target genes [90,91]. To explore the mechanism underlying the osteogenic and angiogenic capability of miR-196a-5p,

TargetScan, a target-predicting website, was used to predict the potential downstream targeted genes of miR-196a-5p. As shown in Fig. 6A, we intersected the target genes related to osteogenesis and angiogenesis through gene ontology (GO) analysis in KOBAS 3.0. Among these target genes, *Hoxa7* belonging to the HOX family of genes was focused. It was reported that *Hoxa7* was important regulators of cell fate and pattern formation during embryogenesis and involved in stem cell differentiation [92]. Previous study has demonstrated that down-regulation of *Hoxa7* is required for cell adhesion and migration on fibronectin using a model in which HL-60 cells are induced to differentiate toward the monocytic lineage with bone marrow stromal-like cells [93]. Also, the study indicated reduction of *Hoxa7* as targets of miR-920 could promote osteogenic differentiation of human bone mesenchymal stem cells in osteoporosis population [94]. Of note, the expression of *Hoxa7* was significantly downregulated after treatment with Akt-exo (Fig. S9A). In contrast, it was clear that the expression of *Hoxa7* was increased after Akt+196a inhibitor-exo stimulation (Fig. S9B). Moreover, *Hoxa7* was significantly downregulated after treatment with Akt extracts in Y-BMSCs (Fig. S9C). In addition, other target genes including TGF-βR3, IGF1 and PDGFRA were positively related to osteogenic and angiogenic differentiation [95–97]. Therefore, *Hoxa7* was considered as the most potential target in osteogenic-related process, and hence selected for further investigation.

Based on the bioinformatics, the binding sites in the 3′-UTR regions of *Hoxa7* were partially complementary with miR-196a-5p (Fig. 6B). The luciferase assay demonstrated that miR-196a-5p mimic transfection could significantly decrease the luciferase activity of *Hoxa7*-WT rather than that of *Hoxa7*-MT (Fig. 6C). *Hoxa7* was significantly increased after *Hoxa7* overexpression plasmids transfection (Fig. S9D). To further clarify the regulatory mechanisms of miR-196a-5p through targeting *Hoxa7*, we co-transfected the *Hoxa7* overexpression plasmids with the miR-196a-5p mimics to observe biological function. As presented in Fig. 6D–H, the qRT-PCR results showed that the expression of osteogenic genes including *Alp*, *Bmp-2*, *Col-1*, *Ocn* and *Runx2* and angiogenesis genes *Ang-1* and *Vegf* (Figs. S9E–9F) was upregulated along with elevated expression of miR-196a-5p, but the function was drastically compromised when the O-BMSCs were co-transfected with *Hoxa7* overexpression plasmids. Moreover, the overexpression of miR-196a-5p could decrease the expression of senescence-related genes *p53*, *p21* and *p16*, but was rescued by the *Hoxa7* overexpression plasmids, which displayed an opposite trend compared to osteogenic genes (Fig. 6I–K). In addition, ALP staining results also indicated that miR-196a-5p could promote the osteogenic differentiation; however, the effect was weakened after the cells had been co-transfected with *Hoxa7* overexpression plasmids (Fig. 6L). Conversely, SA-β-gal staining demonstrated that miR-196a-5p could decrease the positive staining cells, while *Hoxa7*
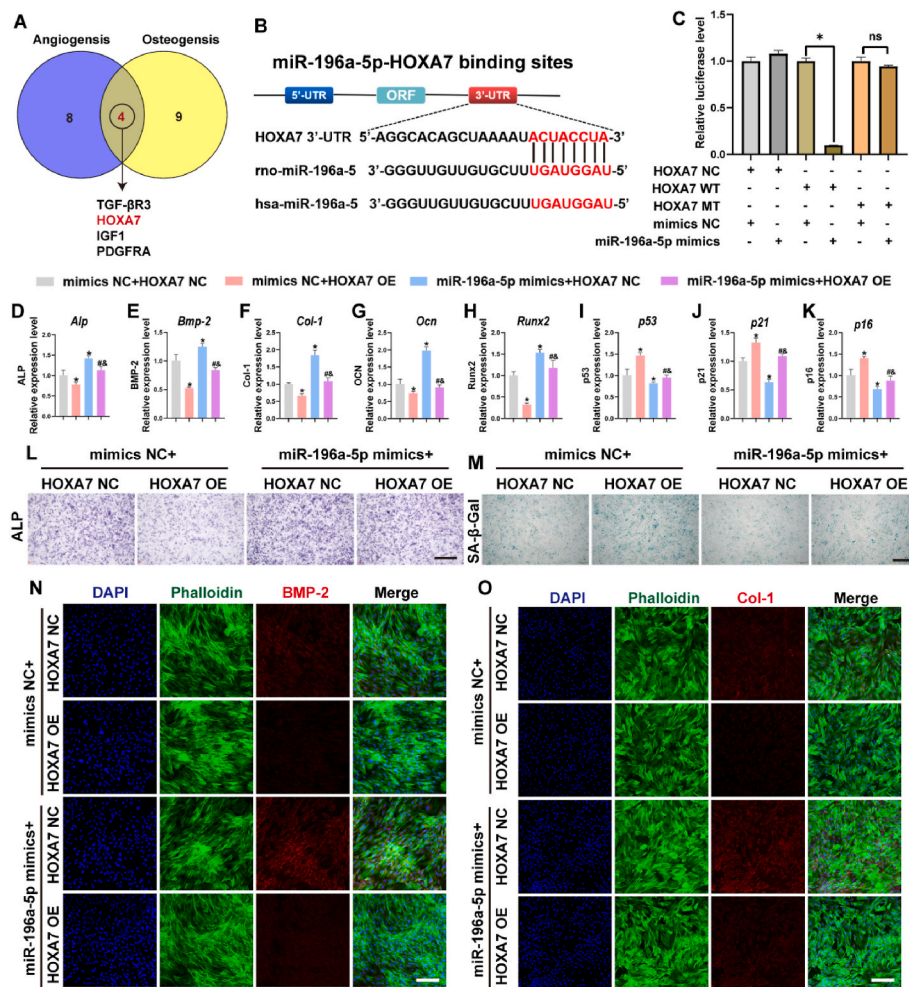

Fig. 6. Exosomal miR-196a-5p mediated osteogenesis of O-BMSCs via targeting *Hoxa7*. (A) Screening of target genes. (B) The predicted binding sites of miR-196a-5p in the 3′-UTR regions of *Hoxa7*. (C) The luciferase assay for miR-196a-5p and *Hoxa7*. (D–L) qRT-PCR analysis of osteogenesis-related genes *Alp* (D), *Bmp-2* (E), *Col-1* (F), *Ocn* (G), *Runx2* (H) and senescence-related genes *p53* (J), *p21* (J) and *p16* (K) for O-BMSCs after different transfections. (L–O) The ALP staining (L), SA-β-Gal staining (M) and the immunofluorescence staining of osteogenesis-related proteins Bmp-2 (N) and Col-1 (O) for O-BMSCs after different transfections.. (*indicates significant differences compared with the group mimics NC + HOXA7 NC; #indicates significant differences compared with the group mimics NC + HOXA7 OE; &indicates significant differences compared with the group miR-196a-5p mimics + HOXA7 NC, $p < 0.05$. Scale bar, 100 μm.)

increased the positive staining cells (Fig. 6M). Moreover, cell immuno-fluorescence staining further confirmed that the expression of osteogenic-related proteins Bmp-2 and Col-1 was significantly increased after the cells had been stimulated by miR-196a-5p mimics; however, the promotional effects were attenuated when the cells were co-transfected with *Hoxa7* overexpression plasmids (Fig. 6N–O). Collectively, all the above results indicated that miR-196a-5p directly targeted *Hoxa7* to regulate the osteogenic-, angiogenic- and senescent-related phenotypes.

2.7. Exosomal miR-196a-5p mediated osteogenesis through activating Hoxa7/MAPK axis

To detect the potential downstream signaling pathway that might be involved in osteogenesis and angiogenesis activated by HOXA7. Using KOBAS 3.0, we performed Kyoto Encyclopedia of Genes and Genomes (KEGG) pathway analysis. Our previous results of the present study demonstrated that Akt extracts could promote osteogenesis of O-BMSCs via activating MAPK pathways. Previous study also showed that p38 and
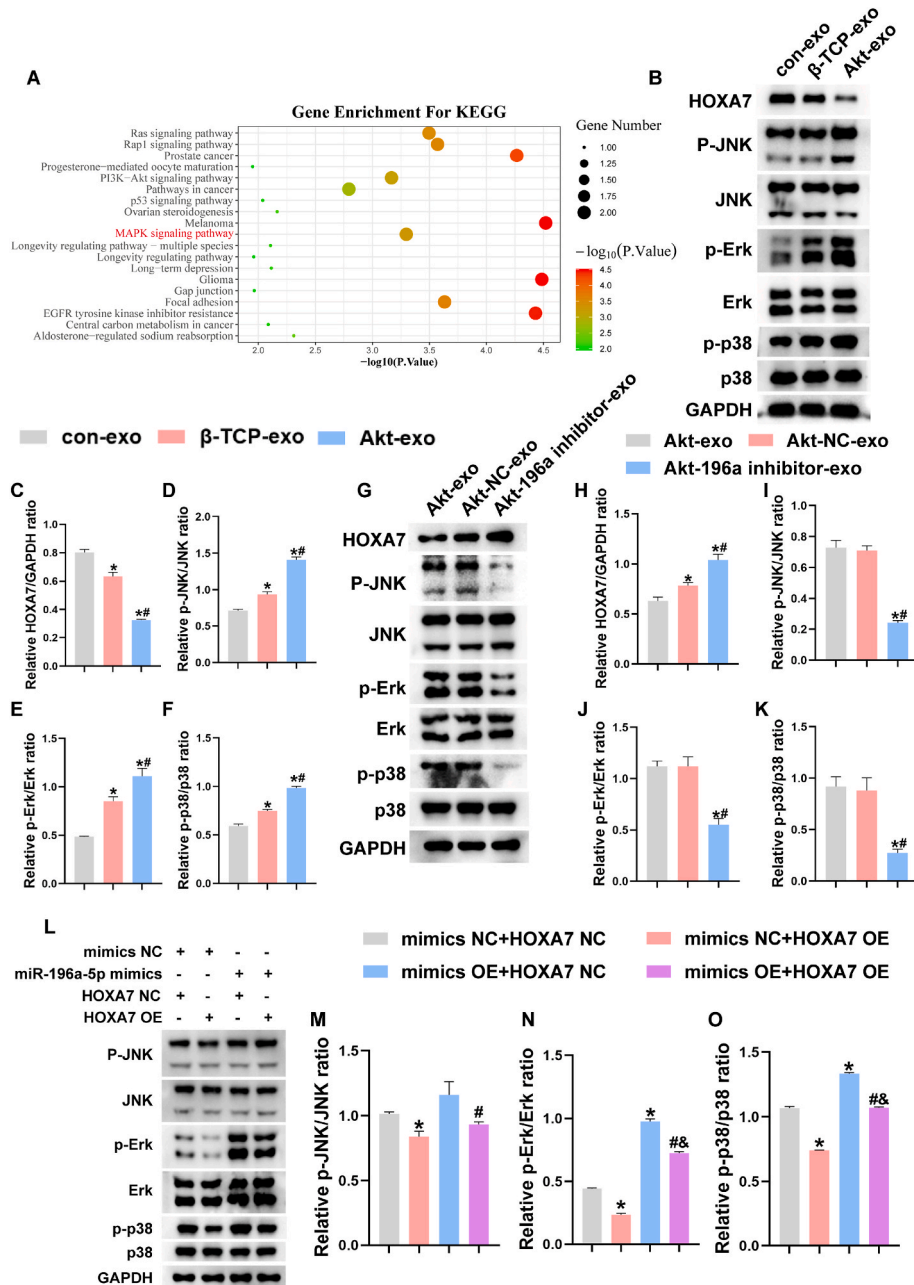

Fig. 7. Exosomal miR-196a-5p mediated osteogenesis of O-BMSCs via targeting *Hoxa7*/MAPK pathways. (A) KEGG analysis of the pathways of target genes. (B) Western blotting assay for proteins expression Hoxa7 and MAPK pathway for O-BMSCs treated with con-exo, β-TCP-exo and Akt-exo. (C–F) The quantitative assay for the ratios of HOXA7/GAPDH (C), p-JNK/JNK (D), p-Erk/Erk (E), p-p38/p38 (F) in different group. (*indicates significant differences compared with con-exo; # indicates significant differences compared with β-TCP-exo. $p < 0.05$.) (G) Western blotting assay for proteins expression Hoxa7 and MAPK pathway for O-BMSCs treated with Akt-exo, Akt + NC-exo and Akt+196a inhibitor-exo. (H–K) The quantitative assay for the ratios of HOXA7/GAPDH (H), p-JNK/JNK (I), p-Erk/Erk (J), p-p38/p38 (K) in different group. (*indicates significant differences compared with Akt-exo; # indicates significant differences compared with Akt + NC-exo. $p < 0.05$.) (L) Western blotting assay for proteins expression of MAPK pathway for O-BMSCs after different transfections.. (*indicates significant differences compared with the group mimics NC + HOXA7 NC; # indicates significant differences compared with the group mimics NC + HOXA7 OE; &indicates significant differences compared with the group miR-196a-5p mimics + HOXA7 NC, $p < 0.05$.)

JNK as potential downstream signaling pathway of *Hoxa7* were involved in osteogenesis of human bone mesenchymal stem cells [94]. Therefore, MAPK was selected (Fig. 7A) among these potential signaling pathways to further investigate the interaction of Hoxa7 and MAPK pathway and clarify exosomal miR-196a-5p regulatory mechanism in O-BMSCs.

The Western blot assay showed that Akt-exo drastically decreased the protein expression of Hoxa7, which might increase the expression of p-p38, p-JNK, and p-Erk (Fig. 7B–F). In contrast, the protein expression of Hoxa7 was significantly increased after treatment with Akt+196a inhibitor-exo, and at the same time the protein expression of p-p38, p-JNK, and p-Erk was downregulated (Fig. 7G–K). The above results suggested that Hoxa7 modulated the MAPK signaling pathway to regulate Akt-exo-mediated osteogenesis. In addition, the results revealed that the protein expression of p-p38, p-JNK, and p-Erk was upregulated when the cells were transfected with miR-196a-5p mimics; however, the promoting effect was attenuated after co-transfecting with Hoxa7 overexpression plasmids (Fig. 7L–O). Collectively, our results demonstrated that exosomal miR-196a-5p mediating Hoxa7/MAPK axis might be an important regulatory mechanism underlying Akt-exo-mediated osteogenesis and angiogenesis.

MAPK signaling as the downstream pathway mediated by exosomes exerts a crucial role in the development of multiple bone-related diseases. Previous study indicated that the exosome derived from BMSCs promote proliferation of osteoblasts to further ameliorate osteoporosis via MAPK signaling pathway [98]. Also, exosomal miR-122-5p blocked the development of osteonecrosis of the femoral head through promoting proliferation of osteoblasts via the RTK/Ras/MAPK signaling pathway [99]. Exosomal miR-196a-5p stimulated by Akt in our present study mediate osteogenesis and rescue senescence by targeting Hoxa7 and then activating MAPK signaling pathway, which was consistent with the previous results of Akt extracts.

2.8. Akt 3D-printed scaffold promotes bone regeneration of aged rats in vivo

Unlike young individuals, senescent niches would increase the pro-inflammatory factors secretion and osteoclast activity, which would bring more difficulties for bone repair [100–102]. Recently, the multifunctional scaffolds fabricated by 3D-printed technique was considered as an ideal strategy in bone tissue engineering due to their controlled
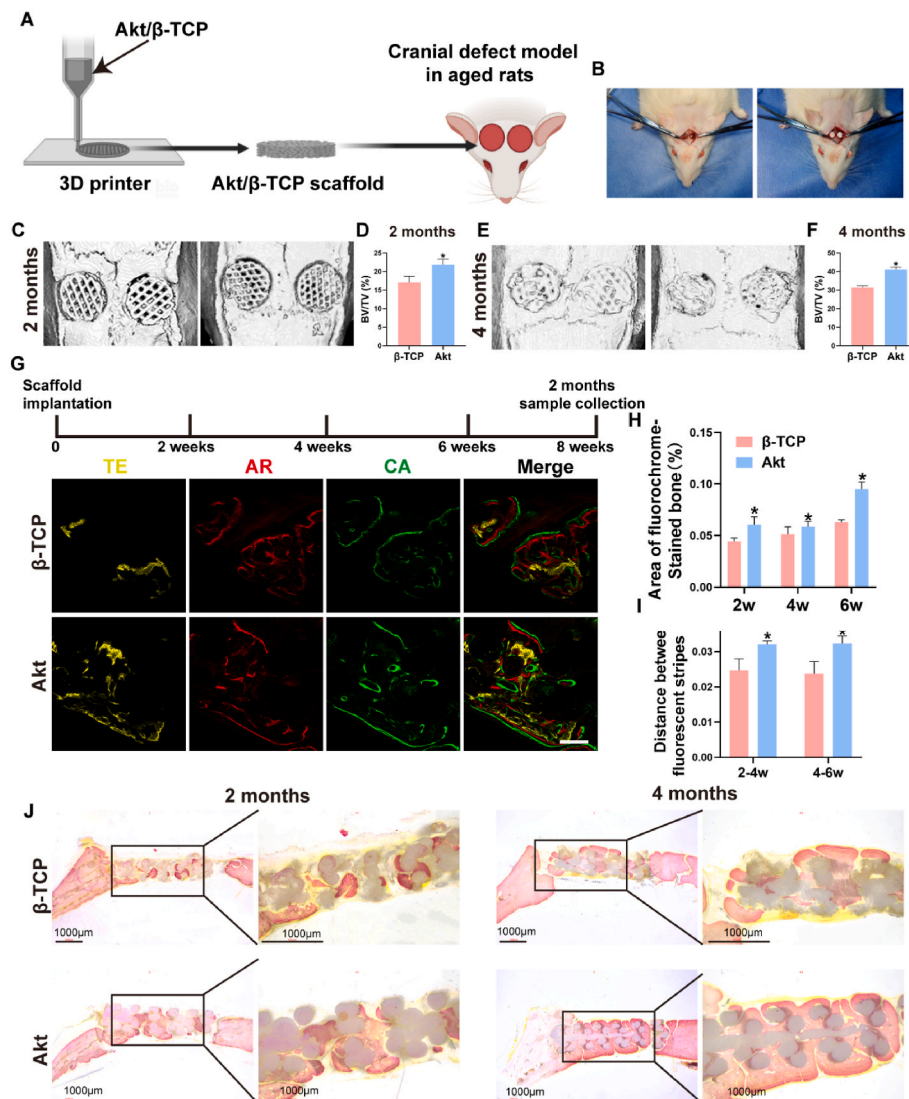
Fig. 8. 3D-printed Akt scaffold promotes bone regeneration of aged rats. (A) Schematic diagram of the construction of Akt or β-TCP scaffold and implantation of cranial defect model of aged rats. (B) Establishment of cranial defect model of aged rats. (C–F) Micro-CT analysis of bone formation at the defect sites (C, E) and its quantification of bone volume/total volume (BV/TV) (D, F) after 2-month and 4-month operation. (G–I) Sequential fluorescent labeling after 2-month operation: (G) fluorescence observation by CLSM, its (H) quantification of stained bone area and (I) distance between stripes. (J) Histological evaluation of the bone formation stained with VG. * indicates significant differences compared with β-TCP, $p < 0.05$.

porosity and enhanced physical and chemical properties [103,104]. Previous study have demonstrated that 3D-printed porous Akt scaffolds could facilitate bone ingrowth and regeneration [105]. Hence, in this study, As shown in Fig. 8A and B, 3D-printed porous Akt or β-TCP scaffolds were prepared and implanted into the cranial defects of aged SD rats to investigate their functions for osteogenesis *in vivo*.

As shown in Fig. 8C–F, micro-CT analysis demonstrated that compared with β-TCP scaffolds, Akt scaffolds presented higher BV/TV values at 2-month and 4-month, showing a preferable osteogenic capability and new bone formation in Akt group. Of note, the 3D-printing scaffolds were not fully degradation until 4-month. The previous study indicated that the degradation of the materials was decreased with the increase of Mg content with time [106]. The other study indicated that Akt powders lost almost two third of its initial volume with the release of Mg ion after 9 weeks implantation [32]. With the degradation of implanted scaffolds, the released Mg ion may also significantly affect the microenvironmental pH associated with greater new bone regeneration. Furthermore, the bone formation was evaluated by sequential fluorescent labeling at week 2, 4 and 6. A rapid start to bone regeneration by Akt scaffolds was evident from the fact that higher bone mineralization was seen in the Akt group at 2 weeks, while less bone development was indicated in the β-TCP group during the same period. Additionally, Akt dramatically increased the amount of new bone growth at week 4 and 6 compared to the β-TCP group. More

significantly, the mineral deposition rate for the Akt group was higher than that in the β-TCP group at week 2–4 and 4-6 post-operation (Fig. 8G–I). Additionally, the 2-month VG data showed that the Akt scaffolds had greater new bone growth into their porosity, whereas the β-TCP group had only a thin layer of new bone surrounding the material (Fig. 8J). After 4-month implantation, both groups all had more new bone formation in the porosity of the scaffolds compared to 2-month (Fig. 8J), while the Akt group induced denser and thicker bone formation than β-TCP group. Taken together, the *in vivo* results demonstrated that 3D-printed Akt scaffolds pronouncedly increased new bone formation than β-TCP scaffolds.

The *in vivo* results displayed that the short-term repair effect either in the Akt group or the β-TCP group was not satisfactory, which might be attributed to the pro-inflammatory and osteoclastic microenvironments. Hence, in the following studies, functional Akt scaffolds were developed to decrease the influence of detrimental factors and accelerate bone regeneration in an aging microenvironment. Secondary, due to the difficulty in degradation, the decalcified samples could not obtain to perform the experiments including HE, Masson and other histological staining. In view of this point, other methods including incorporation of Akt powder into other scaffolds were employed to evaluate the effects of Akt on bone regeneration *in vivo* in the future study. In addition, the experiments about CS 3D printed scaffolds *in vivo* should be performed in the following study.
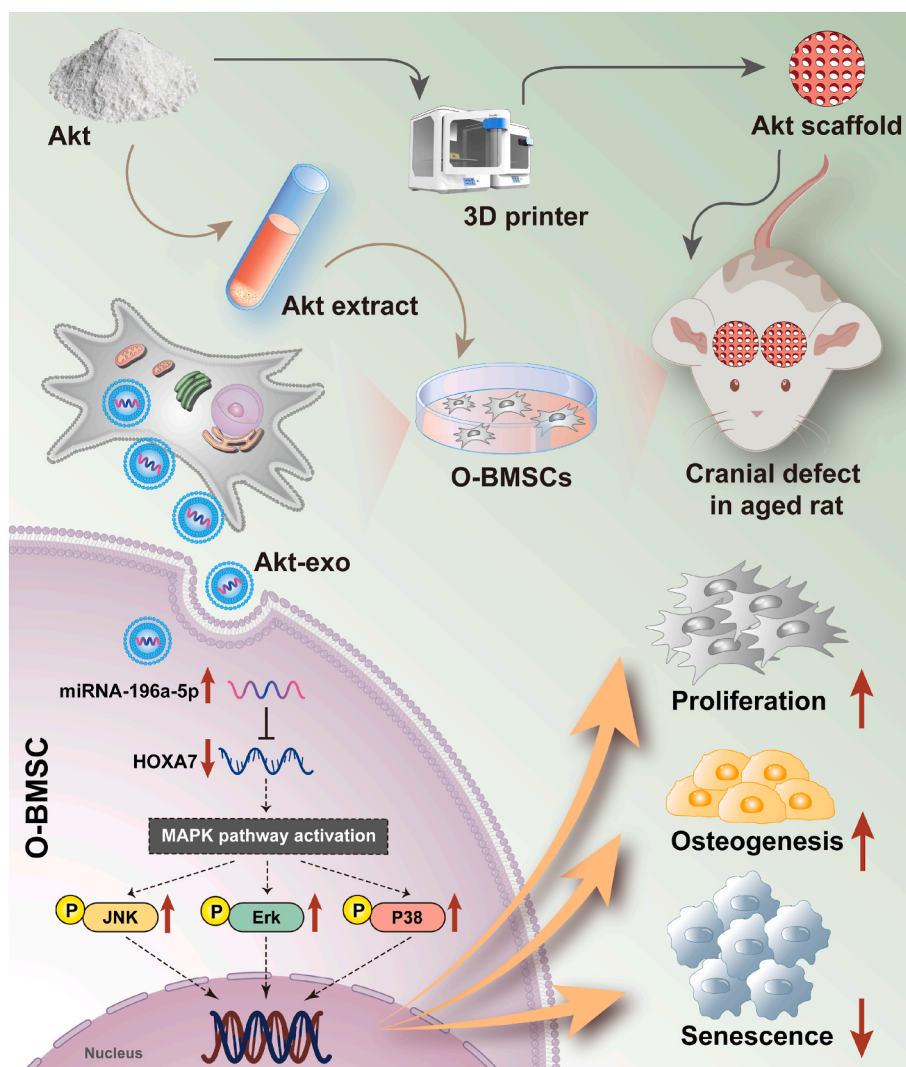

Fig. 9. Schematic diagram depicts the detailed mechanisms involved in Akt-mediated osteogenesis of O-BMSCs through exosomal miR-196a-5p.

3. Conclusion

To sum up, the present study proved that Akt extracts exhibited latent capacities for improving osteogenesis and suppressing the senescence-related phenotype of O-BMSCs *in vitro*. These positive effects might be attributed to the activation of MAPK, including JNK, Erk and p38 signaling pathways. Moreover, Akt biocreamics indirectly facilitated the osteogenic capacity of O-BMSCs by secreting exosomal miR-196a-5p transferred by Akt-exo inhibited the expression of *Hoxa7* and then activated the MAPK signaling pathway to accelerate bone regeneration. The exosomal-miR-196a-5p/*Hoxa7*/MAPK signaling axis might be the potential mechanism of Akt-mediated osteogenesis of O-BMSCs, providing a novel candidate strategy for bone repair in a senescent microenvironment (Fig. 9). Also, the 3D-printed porous Akt scaffolds containing Mg ions were considered as promising scaffolds for bone regeneration in aged individuals.

4. Experimental section

Preparation of Akt, CS and β-TCP powders: Akt powders were synthesized by a sol-gel process using tetraethyl orthosilicate ($(C_2H_5O)_4Si$, TEOS), magnesium nitrate hexahydrate ($Mg(NO_3)_2 \cdot 6H_2O$) and calcium nitrate tetrahydrate ($Ca(NO_3)_2 \cdot 4H_2O$) as raw materials [65]. Briefly, The TEOS was mixed with ethanol and 2 M HNO_3 and hydrolyzed for 45 min under stirring. In continue, $Mg(NO_3)_2 \cdot 6H_2O$ and $Ca(NO_3)_2 \cdot 4H_2O$ were added into the mixture, and were stirred for 5 h at room temperature. Then, the obtained solution was maintained at a constant temperature 75 °C for 24 h and dried at 120 °C for 48 h to obtain the dry gel. The resultant gel was milled and sieved to 250-mesh, transferred into a corundum crucible and sintered at 1200 °C for 3 h. Finally, to ensure the preparation of nanoparticle powder, the resultant powder was milled for 10 h (rotational speed of 250 rpm, ball/powder ratio of 5/1). The CS and β-TCP powders were synthesized by chemical precipitation method [45]. For CS powders, 0.5 M $Ca(NO_3)_2 \cdot 4H_2O$ solution was dripped wisely into the 0.5 M $Na_2SiO_3 \cdot 9H_2O$ solution at room temperature under rigorously stirring with Ca/Si molar ratio of 1.0. For β-TCP powders, 0.5 M $Ca(NO_3)_2 \cdot 4H_2O$ aqueous solution was dripped into 0.5 M $(NH_4)_2HPO_4$ aqueous solution under rigorously stirring with the molar ratio of Ca/P was set at 1.5. The pH value was maintained at approximately 8.0 using ammonium hydroxide aqueous solution. After that, the above mixtures were further stirred for 24 h, and then filtered and washed with deionized water for three times. Finally, the obtained powders were calcined at 800 °C for 2 h to obtain CS and β-TCP powders, respectively.

Preparation and characterization of extracts and scaffolds: The Akt and β-TCP extracts were prepared using the following methods. Briefly, 1g of Akt, CS or β-TCP powders were immersed in 5ml of α-MEM and shaken at 37 °C in an incubator for 24 h. After centrifugation, the samples were filtered using filters (Millipore, 0.22 μm) for sterilization. Inductively coupled plasma atomic emission spectroscopy (ICP-AES; Varian, USA) was used to measure the concentrations of Ca, Mg, and Si in various diluted Akt, CS or β-TCP samples(1/16, 1/32 and 1/64). In addition, for evaluation of the degradation to confirm the effective release of special ions, Akt scaffolds were soaked in Tris-HCL at 37 °C for 1, 4, 7, 10 and 14 days, respectively and the solution was collected at every point. The element including Mg, Si, Ca concentrations of the scaffolds after soaking for different time periods were measured by inductively coupled plasma atomic emission spectroscopy (ICP-AES; Varian, USA). The samples including Akt, CS and β-TCP were determined by fourier transform infrared spectroscopy (FTIR, Bomen MB 100). X-ray diffraction (XRD; Rigaku D/max 2550VB/PC, Japan) was used to characterize the phase composition of Akt, CS and β-TCP samples. For subsequent animal experiments, Akt and β-TCP powders were 3D-printed as porous scaffolds with a height of 3mm and a diameter of 5mm. Scanning electron microscopy (SEM, JEOL, Japan) was used to observe the structures of 3D-printed scaffolds. The μe-pH variations of different material extracts *in vitro* were detected according to the following methods. In brief,

the material powders were firstly immersed into an SBF solutionsn at 37 °C. After centrifugation, the μe-pH values were measured onto the solid-liquid interface at the time points of 15min, 1d, 2d, 3d, 5d and 7d using a pH-meter (Mettler Toledo, Columbus, OH, USA).

Cell culture: O-BMSCs of aged rats (18-month-old) were harvested and cultured as reported previously [107]. Briefly, the bone marrow was rinsed in $10cm^2$ dishes with α-MEM medium after removing the ends of the femur and tibia. The cells were subsequently cultured in α-MEM medium that contained 10% fetal bovine serum (FBS) and 1% penicillin and streptomycin. The O-BMSCs were passaged after achieving a confluence of around 80–90%. The 2-4 passage O-BMSCs were used for the ensuing tests. The Animal Research Committee of Shanghai Ninth People's Hospital, affiliated to Shanghai Jiao Tong University School of Medicine, approved all these trials, including *in vivo* studies.

Cell proliferation: Akt and β-TCP extracts were diluted to gradient concentration degrees (1/2, 1/4, 1/8, 1/16, 1/32, 1/64), and then the optimal concentration of extract was filtered to perform the following studies. The CS extracts were also chosen to culture O-BMSCs in similar ways to exclude the potential influence of released Si ion from the Akt. The Cell Counting Kit-8 assay (CCK-8; Dojindo, Japan) was used to compare the proliferation capacity of O-BMSCs after treating them with different concentrations of Akt and β-TCP extracts or exosomes. Firstly, the cells at a density of 4×10^3 cells per well were seeded in 96-well plates. Then, ELX Ultra microplate reader (BioTek, USA) was used to measure the cells' absorbance value at 450nm. Additionally, the optical density (OD) was calculated to represent the capacity for cell proliferation.

RNA isolation and qRT-PCR analysis: Real-time quantitative reverse transcription-polymerase chain reaction (RT-qPCR) system (Roche LightCycler96, Basel, Switzerland) was applied to measure all the gene expressions of mRNAs and miRNAs. For mRNA, total RNA was isolated from O-BMSCs after different treatments and different types of exosomes using trizol reagent (Takara, Japan). The following mRNA analysis was carried out by reverse transcription of the RNA into complementary cDNA. For miRNA, the total miRNA underwent poly-A tailing and reverse transcription using the miRNA 1st strand cDNA synthesis kit (Accurate Biology, AG, China). Sangon Biotech (Shanghai, China) created the upstream and downstream primers for mRNAs and miRNAs. The real-time detection kit based on TB-Green was used to carry out the real-time PCR. Relative expression levels of genes were calculated and named to the housekeeping genes β-actin and U6 for mRNAs and miRNAs, respectively. All the primers are provided in Supplementary Table 1.

ALP staining and ARS staining: O-BMSCs were cultured in α-MEM medium with a 1/32 concentration of Akt, β-TCP and CS extracts or various exosome types. After being fixed with 4% paraformaldehyde on day 7, cells were dyed using a BCIP/NBT alkaline phosphatase color development kit (Beyotime, Jiangsu, China) following the instructions of manufacturer. ARS staining was also performed to observe the calcium nodule of O-BMSCs after treatment with a 1/32 concentration of Akt extracts or various exosome types. An inverted light microscope (Leica DMI6000B, Solms, Germany) was then used to observe the ALP staining and ARS staining.

SA-β-gal staining: O-BMSCs were cultured in α-MEM medium mixed with 1/32 concentrations of Akt and β-TCP extracts or various exosome types. Using an SA-gal staining kit from Beyotime (Jiangsu, China) to carried out SA-β-Gal staining to observe positive staining cells. Briefly, the cells were stained with an X-gal solution for 24h at 37 °C (no CO_2) after being fixed with 4% formaldehyde at room temperature for 20min. An inverted light microscope (Leica DMI6000B, Solms, Germany) was used to examine the positively stained cells.

Immunofluorescence: O-BMSCs were cultured in a medium containing extract of Akt and β-TCP at a 1/32 concentration or various exosome types. The cells were fixed with 4% paraformaldehyde, permeabilized with 0.1% Triton X-100, and then blocked with 5% BSA for 1h, and the samples were treated with primary Bmp-2 and Col-1 antibodies

overnight at 4 °C. The samples were then purified with PBS and treated with goat-anti-rabbit IgG tagged with Alexa Fluor® 594 for 1h, FITC-phalloidin for 45min, and DAPI for 10min, respectively, in the dark. The protein expressions of several treatment groups were compared using confocal laser-scanning microscopy (CLSM; Leica, Germany).

Transwell assay: The migration capacity of O-BMSCs after treatment with different material extracts was evaluated using Transwell cell culture inserts (8 μm pore size; Corning/Costar, Corning, USA) in 24-well plates. The O-BMSCs were seeded into the upper chamber in 300 μl of serum-free medium while the lower chamber contained 700 μl of complete medium supplemented with 10% FBS and different material extracts. After incubation at 37 °C for 24 h, the cells were fixed with 4% paraformaldehyde for 20 min and stained with crystal violet for 30 min. The cells in the upper chambers were removed and the migrated cells were observed and photographed using an inverted light microscope (Leica DMI6000B, Solms, Germany).

Western blot analysis: RIPA lysis buffer (Invitrogen, USA) containing 1mM phenylmethanesulfonyl fluoride (PMSF) was used to extract the protein from cultured cells. The amount of protein was measured by the PierceTM BCA Protein Assay kit from Thermo Scientific (USA). The proteins were separated in an SDS-PAGE gel and then transferred to a PVDF membrane (0.22 μm, Merck Millipore, USA), blocked with 5% BSA, treated with primary antibodies at 4 °C for an overnight period, and then incubated with a secondary goat anti-rabbit antibody that had been (HRP)-conjugated at 37 °C for 1h. The enhanced chemiluminescence (ECL) substrate kit (Merck Millipore, USA) was then used to identify the proteins, and Image J was used to quantify their expression. The expression was compared to the internal reference value (GAPDH).

Signaling pathway inhibition: SP600125, PD98059 and SB202190, as the inhibitors of JNK, Erk and p38, respectively, were used in the medium supplemented with Akt extracts to indicate the function of these pathways in Akt-mediated osteogenesis. Briefly, O-BMSCs were treated with the above three inhibitors and then stimulated with Akt extracts. Western blot assay was used to measure the protein expression of p-Erk, p-P38 and p-JNK. And the qRT-PCR, ALP staining, SA-β-gal staining and immunofluorescence were also conducted as described above.

Isolation, characterization, and internalization of exosomes: The exosomes were derived from early-passaged O-BMSCs. In brief, the BMSCs were cultured in α-MEM medium containing an optimal concentration of Akt or β-TCP extracts with exosome-free FBS. The supernatants were gathered and purified after 48h. To eliminate cells and cell debris, the medium was centrifuged at 10000g for 30min at 4 °C and at 100000g for 90min to collect the exosome pellets. The amount of protein in the gathered exosomes was detected using a BCA protein assay kit from Thermo Scientific (USA). Western blot analysis was performed to find the exosomal markers CD63, CD81, and Alix. A transmission electron microscope (TEM; Hitachi, Japan) was used to observe the exosomes morphology. The concentration and particle diameter of the separated exosomes were detected by nanoparticle tracking analysis (NTA; NanoSight NS300, Malvern, UK). To analyze the internalization of the exosomes, the different exosomes were labeled with Dil (red fluorescent dye) and then co-cultured with the O-BMSCs. The red fluorescent intensity was determined using Image J to represent internalized exosomes.

Exosomal miRNA sequencing and bioinformatic analyses: Exosomes stimulated by Akt extracts or β-TCP extracts were isolated and purified as previously described. The miRNAs in exosomes were extracted using mirVana miRNA Isolation Kit (Ambion) according to the manufacturer's protocol. 1 μg total RNA of each sample was used for the miRNA library construction using NEBNext Small RNA Library Prep Set for Illumina kit (Cat. No. NEB#E7330S, NEB, USA) following the manufacturer's recommendations. The exosomal miRNA sequencing and analysis were conducted by OE Biotech Co., Ltd. (Shanghai, China). After the significance analysis, differentially expressed genes were selected according to certain criteria (p-value <0.05 and fold change >2). Potential target genes of miRNAs were predicted by databases (TargetScan) and underwent gene ontology (GO) and Kyoto Encyclopedia of Genes and Genomes (KEGG) pathway enrichment analyses by KOBAS 3.0.

Transfection of miRNA mimics or inhibitors and mRNA overexpression plasmids: The specific miR-196a-5p inhibitors or mimics and HOXA7 overexpression plasmids were transfected to further investigate their function in the process of Akt-mediated osteogenesis. The O-BMSCs were treated with the Lipofectamine RNAiMAX transfection reagent carrying the miRNA inhibitor and a negative control. After 6–8 h, the cultured medium was replaced with α-MEM medium containing Akt extracts and exosome-free FBS. After another 48h, the exosomes were collected and purified as described above. In addition, the O-BMSCs were also simultaneously transfected with HOXA7 overexpression plasmids and miR-196a-5p mimics/mimics NC. The functional assays, including qRT-PCR, ALP staining, SA-β-gal staining, and immunofluorescence, were performed as described above.

Luciferase assay: HEK-293T cells were used to perform the dual-luciferase reporter assay. Firstly, plasmids containing different sequences, including Hoxa7 3′ UTR WT and Hoxa7 3′ UTR MT, miR-196a-5p mimics, and NC, were engineered and constructed. After transfecting with different plasmids, Luciferase Assay Kit (GENE, Shanghai, China) was applied to detect the firefly luciferase activities and Renilla luciferase activities. The ratios of firefly luciferase activities to Renilla luciferase activities were recorded to reflect the relative luciferase activity.

Construction of a calvarial defect model: After anesthesia, old rats (18 months) were used to establish an animal model of critical calvarial defects. Bilateral defects of 5mm diameter were created in the calvarium. The old rats were separated into two groups to implant the Akt and β-TCP scaffolds, randomly. After implantation for 2 and 4 months, the calvarial bones of the rats were donated and fixed with 4% paraformaldehyde to perform the following experiments.

Micro-CT: The formation of new bone was evaluated using micro-computed tomography (micro-CT; PerkinElmer Quantum GX, USA) within the defect region. The parameters of the micro-CT were set as follows: 90 kV, 88 μA and 50 μm voxel size. Analyze 12.0 (PerkinElmer) was used to measure and assess the morphology of the cranial bone. To value the new bone formation in the defect area, the rate of new bone volume to tissue volume (BV/TV) was counted.

Sequential fluorescent labeling and VG staining: Tetracycline (TE, 25 mg/kg), alizarin red (AL, 30 mg/kg) and calcein (CA, 20mg/kg) were intraperitoneally injected into the rats at 2-, 4- and 6- week scaffold implantation, and the specimens were obtained and observed at week 8 using the trichromatic sequential fluorescent labeling. CLSM (Leica, Germany) was used to evaluate the fluorescent intensity of these specimens. The intensity of fluorescence-marked images was assessed to indicate bone formation and mineralization at different time points after the operation. VG staining was performed to examine new bone formation under CLSM (Leica, Germany).

Statistics analysis: All data in this study were presented as mean $\pm$ standard deviation (SD). Student's t-test was conducted in SPSS 17.0 software (SPSS Inc., USA). $p < 0.05$ were considered statistically significant.

Credit author statement

Steve GF Shen, K. L. Lin, L. Zhang designed the experiment. X. F, C. C. Pan conducted the biomaterial preparation and testing. L. Qi, J. G. Yan, W.W.Ge and J. Wang performed the experiments and analyzed the data. L. Qi and J. G. Yan wrote the manuscript. All authors have read and approved the final manuscript.

Ethics approval and consent to participate

All the animal care and experimental protocols were performed in agreement with the rules of the Animal Ethical and Experimental

Committee of Shanghai Ninth People's Hospital affiliated to Shanghai Jiao Tong University School of Medicine.

This work does not use human subjects.

Declaration of competing interest

The authors declare no competing financial interests or personal relationships that could have influenced the work reported in this paper.

Acknowledgements

Appendix A. Supplementary data

Supplementary data to this article can be found online at https://doi.org/10.1016/j.bioactmat.2023.10.024.

References

[1] C. López-Otín, M.A. Blasco, L. Partridge, M. Serrano, G. Kroemer, Cell 153 (2013) 1194.
[2] M.A. Goodell, T.A. Rando, Science 350 (2015) 1199.
[3] J. Oh, Y.D. Lee, A.J. Wagers, Nat. Med. 20 (2014) 870.
[4] M.F. Pittenger, A.M. Mackay, S.C. Beck, R.K. Jaiswal, R. Douglas, J.D. Mosca, M. A. Moorman, D.W. Simonetti, S. Craig, D.R. Marshak, Science 284 (1999) 143.
[5] E.P. Paschalis, P. Fratzl, S. Gamsjaeger, N. Hassler, W. Brozek, E.F. Eriksen, F. Rauch, F.H. Glorieux, E. Shane, D. Dempster, A. Cohen, R. Recker, K. Klaushofer, J. bone Miner. Res. Off. J. Am. Soc. Bone Miner. Res. 31 (2016) 347.
[6] N. Baker, L.B. Boyette, R.S. Tuan, Bone 70 (2015) 37.
[7] J. Wu, W. Zhang, Q. Ran, Y. Xiang, J.F. Zhong, S.C. Li, Z. Li, Stem Cell. Int. 2018 (2018), 1540148.
[8] S. Zhou, J.S. Greenberger, M.W. Epperly, J.P. Goff, C. Adler, M.S. Leboff, J. Glowacki, Aging Cell 7 (2008) 335.
[9] Y. Song, H. Wu, Y. Gao, J. Li, K. Lin, B. Liu, X. Lei, P. Cheng, S. Zhang, Y. Wang, J. Sun, L. Bi, G. Pei, ACS Appl. Mater. Interfaces 12 (2020), 16058.
[10] É.R. Oliveira, L. Nie, D. Podstawczyk, A. Allahbakhsh, J. Ratnayake, D.L. Brasil, A. Shavandi, Int. J. Mol. Sci. (2021) 22.
[11] A. Ho-Shui-Ling, J. Bolander, L.E. Rustom, A.W. Johnson, F.P. Luyten, C. Picart, Biomaterials 180 (2018) 143.
[12] G. Ye, F. Bao, X. Zhang, Z. Song, Y. Liao, Y. Fei, V. Bunpetch, B.C. Heng, W. Shen, H. Liu, J. Zhou, H. Ouyang, Nanomedicine (Lond). 15 (2020) 1995.
[13] S. Yamanaka, Cell Stem Cell 27 (2020) 523.
[14] C.R. Harrell, B.S. Markovic, C. Fellabaum, A. Arsenijevic, V. Volarevic, Biomed. Pharmacother. 109 (2019) 2318.
[15] M. Qu, X. Jiang, X. Zhou, C. Wang, Q. Wu, L. Ren, J. Zhu, S. Zhu, P. Tebon, W. Sun, A. Khademhosseini, Adv. Healthcare Mater. 9 (2020), e1901714.
[16] M. Qasim, D.S. Chae, N.Y. Lee, J. Biomed. Mater. Res. 108 (2020) 394.
[17] S.H. Lin, W.J. Zhang, X.Q. Jiang, Chinese J. Dent. Res. Off. J. Sci. Sect. Chinese Stomatol. Assoc. 22 (2019) 93.
[18] Z. Chen, W. Zhang, M. Wang, L.J. Backman, J. Chen, ACS Biomater. Sci. Eng. 8 (2022) 2321.
[19] B. Kołodziejska, N. Stępień, J. Kolmas, Int. J. Mol. Sci. (2021) 22.
[20] Z. Saidak, E. Haÿ, C. Marty, A. Barbara, P.J. Marie, Aging Cell 11 (2012) 467.
[21] S. Galli, M. Stocchero, M. Andersson, J. Karlsson, W. He, T. Lilin, A. Wennerberg, R. Jimbo, Osteoporos. Int. 28 (2017) 2195.
[22] R. Parai, S. Bandyopadhyay-Ghosh, J. Mech. Behav. Biomed. Mater. 96 (2019) 45–52.
[23] J.W. Nieves, Nat. Rev. Endocrinol. 10 (2014) 255–256.
[24] H. Qin, J. Weng, B. Zhou, W. Zhang, G. Li, Y. Chen, T. Qi, Y. Zhu, F. Yu, H. Zeng, Biol. Trace Elem. Res. 201 (2023) 2823–2842.
[25] F. Hohenbild, M. Arango Ospina, S.I. Schmitz, A. Moghaddam, A.R. Boccaccini, F. Westhauser, Int. J. Mol. Sci. 22 (2021), 12703.
[26] K. Bavya Devi, V. Lalzawmliana, M. Saidivya, V. Kumar, M. Roy, S. Kumar Nandi, Chem. Rec. 22 (2022), e202200136.
[27] X. Dong, H. Li, L. E, J. Cao, B. Guo, RSC Adv. 9 (2019), 25462.
[28] T. Tian, Y. Han, B. Ma, C. Wu, J. Chang, J. Mater. Chem. B 3 (2015) 6773.
[29] F. Wang, X. Wang, K. Ma, C. Zhang, J. Chang, X. Fu, Wound repair Regen. Off. Publ. Wound Heal. Soc. [and] Eur. Tissue Repair Soc. 28 (2020) 16.
[30] Y. Han, Y. Li, Q. Zeng, H. Li, J. Peng, Y. Xu, J. Chang, J. Mater. Chem. B 5 (2017) 3315.
[31] N.E. Putra, K.G.N. Borg, P.J. Diaz-Payno, M.A. Leeflang, M. Klimopoulou, P. Taheri, J.M.C. Mol, L.E. Fratila-Apachitei, Z. Huan, J. Chang, J. Zhou, A. A. Zadpoor, Acta Biomater. 148 (2022) 355.
[32] W. Liu, T. Wang, X. Zhao, X. Dan, W.W. Lu, H. Pan, Bioact. Mater. 1 (2016) 151.
[33] J. Cui, L. Xia, K. Lin, X. Wang, J. Mater. Chem. B 9 (2021) 9505.
[34] R.I. Shader, Clin. Therapeut. 36 (2014) 817.
[35] J.S. Schorey, Y. Cheng, P.P. Singh, V.L. Smith, EMBO Rep. 16 (2015) 24.
[36] Z.-C. Hao, J. Lu, S.-Z. Wang, H. Wu, Y.-T. Zhang, S.-G. Xu, Cell Prolif. 50 (2017).
[37] G. Raposo, W. Stoorvogel, J. Cell Biol. 200 (2013) 373.
[38] S. Mathivanan, H. Ji, R.J. Simpson, J. Proteomics 73 (2010) 1907.
[39] Y. Zha, Y. Li, T. Lin, J. Chen, S. Zhang, J. Wang, Theranostics 11 (2021) 397.
[40] K. Nan, Y. Zhang, X. Zhang, D. Li, Y. Zhao, Z. Jing, K. Liu, D. Shang, Z. Geng, L. Fan, Stem Cell Res. Ther. 12 (2021) 331.
[41] Y. Zhang, Y. Xie, Z. Hao, P. Zhou, P. Wang, S. Fang, L. Li, S. Xu, Y. Xia, ACS Appl. Mater. Interfaces 13 (2021), 18472.
[42] A. Liu, D. Lin, H. Zhao, L. Chen, B. Cai, K. Lin, S.G. Shen, Biomaterials 272 (2021), 120718.
[43] D.B. Patel, K.M. Gray, Y. Santoram, T.N. Lamichhane, K.M. Stroka, S.M. Jay, Bioeng. Transl. Med. 2 (2017) 170.
[44] W. Liu, L. Li, Y. Rong, D. Qian, J. Chen, Z. Zhou, Y. Luo, D. Jiang, L. Cheng, S. Zhao, F. Kong, J. Wang, Z. Zhou, T. Xu, F. Gong, Y. Huang, C. Gu, X. Zhao, J. Bai, F. Wang, W. Zhao, L. Zhang, X. Li, G. Yin, J. Fan, W. Cai, Acta Biomater. 103 (2020) 196.
[45] L. Liu, F. Yu, L. Li, L. Zhou, T. Zhou, Y. Xu, K. Lin, B. Fang, L. Xia, Acta Biomater. 119 (2021) 444.
[46] A. M S, S. Jaiswal, A. Dubey, D. Lahiri, A.K. Das, J. Biomed. Mater. Res. 109 (2021) 1479.
[47] M.M. Belluci, T. Schoenmaker, C. Rossa-Junior, S.R. Orrico, T.J. de Vries, V. Everts, J. Nutr. Biochem. 24 (2013) 1488.
[48] S. Castiglioni, A. Cazzaniga, W. Albisetti, J.A.M. Maier, Nutrients 5 (2013) 3022.
[49] Y. Zhu, S. Zhao, L. Cheng, Z. Lin, M. Zeng, Z. Ruan, B. Sun, Z. Luo, Y. Tang, H. Long, J. Orthop. Res. 40 (2022) 1563.
[50] W. Liu, X. Dan, W.W. Lu, X. Zhao, C. Ruan, T. Wang, X. Cui, X. Zhai, Y. Ma, D. Wang, W. Huang, H. Pan, ACS Appl. Bio Mater. 11 (2019) 9557.
[51] H. Lin, J. Sohn, H. Shen, M.T. Langhans, R.S. Tuan, Biomaterials 203 (2019) 96.
[52] D. Saul, S. Khosla, Endocr. Rev. 43 (2022) 984.
[53] W.H. Cheung, T. Miclau, S.K.-H. Chow, F.F. Yang, V. Alt, Injury 47 (Suppl 2) (2016) S21.
[54] J.N. Farr, S. Khosla, Bone 121 (2019) 121.
[55] J.S. Fernandes, P. Gentile, R.A. Pires, R.L. Reis, P. V Hatton, Acta Biomater. 59 (2017) 2.
[56] H. Ma, C. Feng, J. Chang, C. Wu, Acta Biomater. 79 (2018) 37.
[57] H. Shao, X. Ke, A. Liu, M. Sun, Y. He, X. Yang, J. Fu, Y. Liu, L. Zhang, G. Yang, S. Xu, Z. Gou, Biofabrication 9 (2017), 25003.
[58] Y. Wen, S. Xun, M. Haoye, S. Baichuan, C. Peng, L. Xuejian, Z. Kaihong, Y. Xuan, P. Jiang, L. Shibi, Biomater. Sci. 5 (2017) 1690.
[59] M. Rondanelli, M.A. Faliva, A. Tartara, C. Gasparri, S. Perna, V. Infantino, A. Riva, G. Petrangolini, G. Peroni, Biometals an Int. J. role Met. ions Biol. Biochem. 34 (2021) 715.
[60] J. Zhang, L. Tang, H. Qi, Q. Zhao, Y. Liu, Y. Zhang, Adv. Healthcare Mater. 8 (2019), e1901030.
[61] M. Nabiyouni, T. Brückner, H. Zhou, U. Gbureck, S.B. Bhaduri, Acta Biomater. 66 (2018) 23.
[62] M. Barbagallo, N. Veronese, L.J. Dominguez, Nutrients (2021) 13.
[63] Y. Xu, C. Xu, L. He, J. Zhou, T. Chen, L. Ouyang, X. Guo, Y. Qu, Z. Luo, D. Duan, Bioact. Mater. 16 (2022) 271.
[64] D. Qi, J. Su, S. Li, H. Zhu, L. Cheng, S. Hua, X. Yuan, J. Jiang, Z. Shu, Y. Shi, J. Xiao, Biomater. Adv. 136 (2022), 212759.
[65] L. Xia, Z. Yin, L. Mao, X. Wang, J. Liu, X. Jiang, Z. Zhang, K. Lin, J. Chang, B. Fang, Sci. Rep. 6 (2016), 22005.
[66] M. Wu, G. Chen, Y.-P. Li, Bone Res 4 (2016), 16009.
[67] C. Thouverey, J. Caverzasio, BoneKEy Rep. 4 (2015) 711.
[68] Y. Hu, Y. Wang, T. Chen, Z. Hao, L. Cai, J. Li, Oxid. Med. Cell. Longev. 2021 (2021), 6324912.
[69] T. Liu, W. Hu, X. Zou, J. Xu, S. He, L. Chang, X. Li, Y. Yin, M. Tian, Z. Li, J. Zhou, X. Jiang, S. Chen, Stem Cell. Int. 2020 (2020), 8852307.
[70] K. Agarwal, M. Saji, S.M. Lazaroff, A.F. Palmer, M.D. Ringel, M.E. Paulaitis, Langmuir 31 (2015) 5440.
[71] L. Chen, P. Guo, Y. He, Z. Chen, L. Chen, Y. Luo, L. Qi, Y. Liu, Q. Wu, Y. Cui, F. Fang, X. Zhang, T. Song, H. Guo, Cell Death Dis. 9 (2018) 513.
[72] W. Wu, J. Liu, C. Yang, Z. Xu, J. Huang, J. Lin, Brain Res. Bull. 163 (2020) 84.
[73] C. Li, D.-R. Liu, G.-G. Li, H.-H. Wang, X.-W. Li, W. Zhang, Y.-L. Wu, L. Chen, World J. Gastroenterol. 21 (2015) 6215.
[74] L. Fan, P. Guan, C. Xiao, H. Wen, Q. Wang, C. Liu, Y. Luo, L. Ma, G. Tan, P. Yu, L. Zhou, C. Ning, Bioact. Mater. 6 (2021) 2754.
[75] Y. Hu, X. Li, Q. Zhang, Z. Gu, Y. Luo, J. Guo, X. Wang, Y. Jing, X. Chen, J. Su, Bioact. Mater. 6 (2021) 2905.
[76] Y. Shi, X. Kang, Y. Wang, X. Bian, G. He, M. Zhou, K. Tang, Med. Sci. Monit. Int. Med. J. Exp. Clin. Res. 26 (2020), e923328.
[77] L. Liu, Y. Liu, C. Feng, J. Chang, R. Fu, T. Wu, F. Yu, X. Wang, L. Xia, C. Wu, B. Fang, Biomaterials 192 (2019) 523.

[78] Y. Xiong, L. Chen, C. Yan, W. Zhou, T. Yu, Y. Sun, F. Cao, H. Xue, Y. Hu, D. Chen, B. Mi, G. Liu, J. Nanobiotechnol. 18 (2020) 66.

[79] R. Li, D. Li, H. Wang, K. Chen, S. Wang, J. Xu, P. Ji, Stem Cell Res. Ther. 13 (2022) 149.

[80] Y. Feng, P. Wan, L. Yin, X. Lou, J. Microbiol. Biotechnol. 30 (2020) 448.

[81] H. Long, B. Sun, L. Cheng, S. Zhao, Y. Zhu, R. Zhao, J. Zhu, DNA Cell Biol. 36 (2017) 715.

[82] Y.-F. Luo, X.-X. Wan, L.-L. Zhao, Z. Guo, R.-T. Shen, P.-Y. Zeng, L.-H. Wang, J.-J. Yuan, W.-J. Yang, C. Yue, Z.-H. Mo, Aging 13 (2020) 1186.

[83] Q. Lu, H. Qin, H. Tan, C. Wei, X. Yang, J. He, W. Liang, J. Li, BioMed Res. Int. 2021 (2021), 5576023.

[84] E.C. Tuysuz, U. Ozbey, S. Gulluoglu, A. Kuskucu, F. Sahin, O.F. Bayrak, Dev. Biol. 478 (2021) 212.

[85] B. Wang, P. Yu, T. Li, Y. Bian, X. Weng, Mol. Med. Rep. 12 (2015) 7447.

[86] U. Styrkarsdottir, O.A. Stefansson, K. Gunnarsdottir, G. Thorleifsson, S.H. Lund, L. Stefansdottir, K. Juliusson, A.B. Agustsdottir, F. Zink, G.H. Halldorsson, E. V Ivarsdottir, S. Benonisdottir, H. Jonsson, A. Gylfason, K. Norland, K. Trajanoska, C.G. Boer, L. Southam, J.C.S. Leung, N.L.S. Tang, T.C.Y. Kwok, J.S.W. Lee, S. C. Ho, I. Byrjalsen, J.R. Center, S.H. Lee, J.-M. Koh, L.S. Lohmander, L.T. Ho-Pham, T. V Nguyen, J.A. Eisman, J. Woo, P.-C. Leung, J. Loughlin, E. Zeggini, C. Christiansen, F. Rivadeneira, J. van Meurs, A.G. Uitterlinden, B. Mogensen, H. Jonsson, T. Ingvarsson, G. Sigurdsson, R. Benediktsson, P. Sulem, I. Jonsdottir, G. Masson, H. Holm, G.L. Norddahl, U. Thorsteinsdottir, D.F. Gudbjartsson, K. Stefansson, Nat. Commun. 10 (2019) 2054.

[87] Y. Wang, S. Zhang, H. Yang, Y. Cao, D. Yu, Y. Zhao, Y. Cao, Cell Tissue Res. 390 (2022) 245.

[88] L. Zhang, H. Xie, S. Li, J. Bone Miner. Metabol. 38 (2020) 794.

[89] Y. Takafuji, K. Tatsumi, N. Kawao, K. Okada, M. Muratani, H. Kaji, Calcif. Tissue Int. 108 (2021) 364.

[90] B. Liu, J. Li, M.J. Cairns, Briefings Bioinf. 15 (2014) 1.

[91] B.T. Moore, P. Xiao, MicroRNA 2 (2013) 20.

[92] R.A. da Silva, G.M. Fuhler, V.T. Janmaat, C.J. da C Fernandes, G. da Silva Feltran, F.A. Oliveira, A.A. Matos, R.C. Oliveira, M.R. Ferreira, W.F. Zambuzzi, M. P. Peppelenbosch, Bone 125 (2019) 74.

[93] P. Leroy, F. Berto, I. Bourget, B. Rossi, J. Leukoc. Biol. 75 (2004) 680.

[94] J.-P. Zha, X.-Q. Wang, J. Di, J. Orthop. Surg. Res. 15 (2020) 254.

[95] M. Toledano-Osorio, E. de Luna-Bertos, M. Toledano, F.J. Manzano-Moreno, E. García-Recio, C. Ruiz, R. Osorio, M. Sanz, J. Periodontal. Res. 58 (2023) 296.

[96] J. Yan, J.W. Herzog, K. Tsang, C.A. Brennan, M.A. Bower, W.S. Garrett, B. R. Sartor, A.O. Aliprantis, J.F. Charles, Proc. Natl. Acad. Sci. U.S.A. 113 (2016) E7554.

[97] A. Julien, S. Perrin, E. Martínez-Sarrà, A. Kanagalingam, C. Carvalho, M. Luka, M. Ménager, C. Colnot, J. bone Miner. Res. Off. J. Am. Soc. Bone Miner. Res. 37 (2022) 1545.

[98] P. Zhao, L. Xiao, J. Peng, Y.-Q. Qian, C.-C. Huang, Eur. Rev. Med. Pharmacol. Sci. 22 (2018) 3962.

[99] W. Liao, Y. Ning, H.-J. Xu, W.-Z. Zou, J. Hu, X.-Z. Liu, Y. Yang, Z.-H. Li, Clin. Sci. (Lond). 133 (2019) 1955.

[100] R. Bogeska, A.-M. Mikecin, P. Kaschutnig, M. Fawaz, M. Büchler-Schäff, D. Le, M. Ganuza, A. Vollmer, S. V Paffenholz, N. Asada, E. Rodriguez-Correa, F. Frauhammer, F. Buettner, M. Ball, J. Knoch, S. Stäble, D. Walter, A. Petri, M. J. Carreño-Gonzalez, V. Wagner, B. Brors, S. Haas, D.B. Lipka, M.A.G. Essers, V. Weru, T. Holland-Letz, J.-P. Mallm, K. Rippe, S. Krämer, M. Schlesner, S. McKinney Freeman, M.C. Florian, K.Y. King, P.S. Frenette, M.A. Rieger, M. D. Milsom, Cell Stem Cell 29 (2022) 1273.

[101] A. Salhotra, H.N. Shah, B. Levi, M.T. Longaker, Nat. Rev. Mol. Cell Biol. 21 (2020) 696.

[102] T.H. Ambrosi, O. Marecic, A. McArdle, R. Sinha, G.S. Gulati, X. Tong, Y. Wang, H. M. Steininger, M.Y. Hoover, L.S. Koepke, M.P. Murphy, J. Sokol, E.Y. Seo, R. Tevlin, M. Lopez, R.E. Brewer, S. Mascharak, L. Lu, O. Ajanaku, S.D. Conley, J. Seita, M. Morri, N.F. Neff, D. Sahoo, F. Yang, I.L. Weissman, M.T. Longaker, C. K.F. Chan, Nature 597 (2021) 256.

[103] Y. Feng, S. Zhu, D. Mei, J. Li, J. Zhang, S. Yang, S. Guan, Curr. Drug Deliv. 18 (2021) 847.

[104] S.Y. Hann, H. Cui, T. Esworthy, X. Zhou, S.-J. Lee, M.W. Plesniak, L.G. Zhang, Acta Biomater. 123 (2021) 263.

[105] A. Dasan, J. Kraxner, L. Grigolato, G. Savio, H. Elsayed, D. Galusek, E. Bernardo, J. Funct. Biomater. 13 (2022).

[106] C. Wu, J. Chang, J. Biomed. Mater. Res. B Appl. Biomater. 83 (2007) 153.

[107] L. Qi, W. Ge, C. Pan, W. Jiang, D. Lin, L. Zhang, Front. Bioeng. Biotechnol. 10 (2022), 1090914.

Lei Qi[1], Xin Fang[1], Jinge Yan[1], Cancan Pan, Weiwen Ge, Jing Wang
Department of Oral & Cranio-Maxillofacial Surgery, Shanghai Ninth People's Hospital, College of Stomatology, Shanghai Jiao Tong University School of Medicine, 200011, PR China
National Clinical Research Center for Oral Diseases, 200011, PR China
Shanghai Key Laboratory of Stomatology & Shanghai Research Institute of Stomatology, Shanghai, 200011, PR China

Steve GF. Shen[**]
Department of Oral & Cranio-Maxillofacial Surgery, Shanghai Ninth People's Hospital, College of Stomatology, Shanghai Jiao Tong University School of Medicine, PR China
National Clinical Research Center for Oral Diseases, PR China
Shanghai Key Laboratory of Stomatology & Shanghai Research Institute of Stomatology, Shanghai, 200011, PR China
Shanghai University of Medicine and Health Sciences, Shanghai, 201318, PR China

Kaili Lin[*], Lei Zhang[***]
Department of Oral & Cranio-Maxillofacial Surgery, Shanghai Ninth People's Hospital, College of Stomatology, Shanghai Jiao Tong University School of Medicine, PR China
National Clinical Research Center for Oral Diseases, PR China
Shanghai Key Laboratory of Stomatology & Shanghai Research Institute of Stomatology, Shanghai, 200011, PR China

[**] Corresponding author. Department of Oral and Cranio-maxillofacial Surgery, Shanghai Ninth People's Hospital, School of Stomatology, Shanghai Jiao Tong University, Shanghai, PR China.

[*] Corresponding author. Department of Oral and Cranio-maxillofacial Surgery, Shanghai Ninth People's Hospital, School of Stomatology, Shanghai Jiao Tong University, Shanghai, PR China.

[***] Corresponding author. Department of Oral and Cranio-maxillofacial Surgery, Shanghai Ninth People's Hospital, School of Stomatology, Shanghai Jiao Tong University, Shanghai, PR China.
E-mail address: shengf@sumhs.edu.cn (S.GF. Shen).
E-mail addresses: lklecnu@aliyun.com, linkaili@sjtu.edu.cn (K. Lin), oral66@126.com (L. Zhang).

[1] These authors contributed equally to this work.